Master's Thesis

Effects of Dopants on Wetting and Structure of Confined Chromonic Liquid Crystals

Hyesong Lee

Department of Physics

Graduate School of UNIST

2019

Effects of Dopants on Wetting and Structure of Confined Chromonic Liquid Crystals

Hyesong Lee

Department of Physics

Graduate School of UNIST

Effects of Dopants on Wetting and Structure of Confined Chromonic Liquid Crystals

A thesis
submitted to the Graduate School of UNIST
in partial fulfillment of the
requirements for the degree of
Master of Science

Hyesong Lee

12/04/2018 of submission

Approved by

Advisor
Joonwoo Jeong

Effects of Dopants on Wetting and Structure of Confined Chromonic Liquid Crystals

Hyesong Lee

This certifies that the thesis of Hyesong Lee is approved.

12/04/2018 of submission

signature

Advisor: Joonwoo Jeong

signature

Joonwoo Jeong: Thesis Committee Member #1

signature

Chae Un Kim: Thesis Committee Member #2

signature

So Youn Kim: Thesis Committee Member #3

Abstract

We report on the effects of poly(ethylene glycol) (PEG) doping on the wetting behavior and director configuration of lyotropic chromonic liquid crystals confined in cylinders. First, we investigate how nematic phase's nucleation site is affected by the polymer dopant during the phase transition from the isotropic to the nematic phase. Without the dopant, the SSY's nematic phase nucleates on the glass confining wall, which leads to complete wetting of the nematic phase on the glass. Surprisingly, we find that the minute amount of doping is enough to change the wetting behavior from complete wetting to non-wetting. In PEG-doped confined SSY, the nematic phase does not nucleate on the glass but in bulk as droplets during phase transition. We propose that the PEG adsorption induces the wetting behavior change. Second, we find that PEG-doped SSY forms the double-twist (DT) director configuration in a cylinder as in the pure case but with decreased twist angle and unprecedented domain wall-like defects. The first suggestion to explain these changes is that the PEG induces changes in elastic moduli, especially decreased saddle-splay elastic modulus. However, through energy estimation of the DT structure and accompanying defects, we find the required changes in elastic moduli seem implausible considering the minuscule amount of the dopant. Instead, we conclude that the added PEG leads nematic SSY to have metastable DT configuration; heterogeneity in the observed twist angles and an inconsistent number ratio of two kinds of defects support this scenario. Additionally, it is noteworthy that the changed wetting behavior can facilitate the formation of the metastable states.

Contents

List of Figures

List of Tables

Explanation of terms and abbreviations

LCLC- Lyotropic Chromonic Liquid Crystal

SSY- Sunset Yellow

LC- Liquid Crystal

PEG- Poly(ethylene glycol)

MW- Molecular Weight

APTES- (3-Aminopropyl)triethoxysilane

DT- Double-twist

XPS- X-ray Photoelectron Spectroscopy

I Introduction

1.1. Lyotropic Chromonic Liquid Crystals

Lyotropic chromonic liquid crystals (LCLCs) are composed of disk-like molecules and water. The molecules are found in dyes, drugs, nucleic acids, antibiotics, etc. [1]–[4] When the disk-like molecules are dissolved in water, they stack face-to-face due to non-covalent attraction induced by the molecule's hydrophobic center and hydrophilic periphery like the representative of LCLCs, Sunset Yellow (SSY) in the figure 1-1. This molecules' stacking property is called "chromonic" which reflects birefringence and unique elasticity of LCLCs. If the SSYs are dissolved high enough, then the molecules stack more to make aggregates. The simplest liquid-crystalline phase, the nematic phase forms when the aggregates get to have an orientational order such as z-direction seen in the scheme of the figure 1-1. The "Lyotropic" means the phase is dependent on concentration and temperature. The phases of LCLCs are explained in the next section.

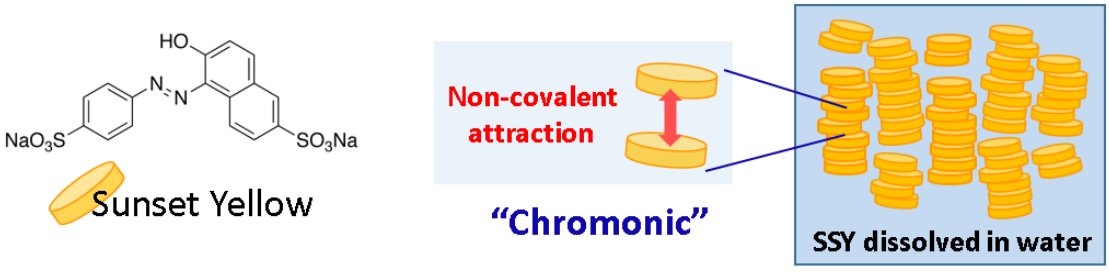

Figure 1- 1. Molecular structure of Sunset Yellow (left), Scheme for "chromonic" term meaning (middle), Scheme of the nematic phase of LCLCs (right), The SSY molecular scheme is from Sigma Aldrich.

1.2. Phases of LCLCs

See the phase diagram of SSY [5] in figure 1-2. There are three phases: isotropic (I), nematic (N), and columnar (C) phase. To illustrate each phase, the isotropic phase is formed when the molecules are dissolved enough not to make aggregates, instead, the short stacks of molecules are dispersed randomly and the isotropic phase is like a normal liquid unlike the liquid crystals (LC). If the molecules are dissolved in water more to make aggregates, then they become to have an orientational order and form the nematic phase. If the aggregates get longer over the extent of the nematic phase, they get closer and build hexagonal columns like a cross-section of a hive. This is how the columnar phase forms.

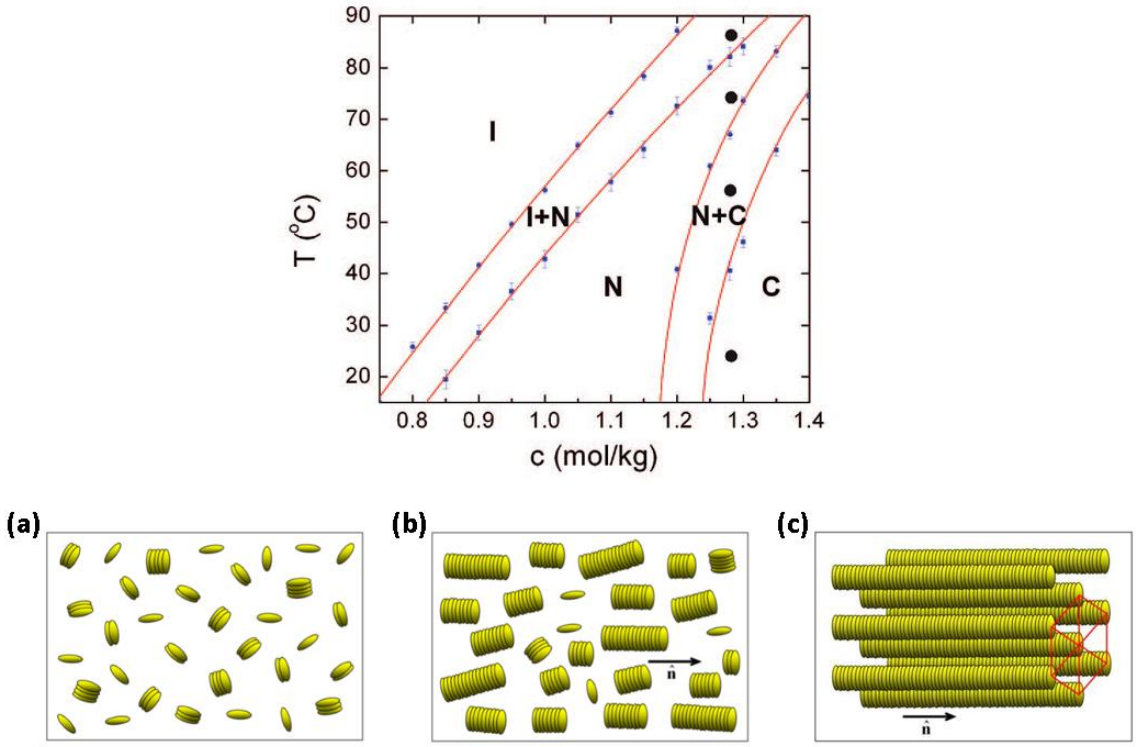

Figure 1- 2. Phase diagram of SSY. [5] The scheme of the SSY phases [58] is (a) Isotropic phase, (b) Nematic phase, and (c) Columnar phase. $\hat{\boldsymbol{n}}$ denotes the direction of average orientational order in the nematic and the columnar phases.

As seen in the figure 1-3, the phase becomes more ordered for a fixed concentration, e.g. 30.0wt%, as the temperature cools. In the same way, as the concentration goes higher for the same temperature, the phase changes from isotropic to nematic and even to columnar phase. Though it is the first order phase transition, there are broad-ranged coexistent phases because of the poly-disperse size distribution of LCLCs. [5] As the system enters into the coexistence phase, a new phase nucleates out of a dominant phase and grows further according to the temperature condition. The experimental pictures in the figure 1-3 are taken under cross polarizers, therefore black region means the isotropic phase or LC region aligning parallel or perpendicular to polarizers. Appeared in red regions are LC phases.

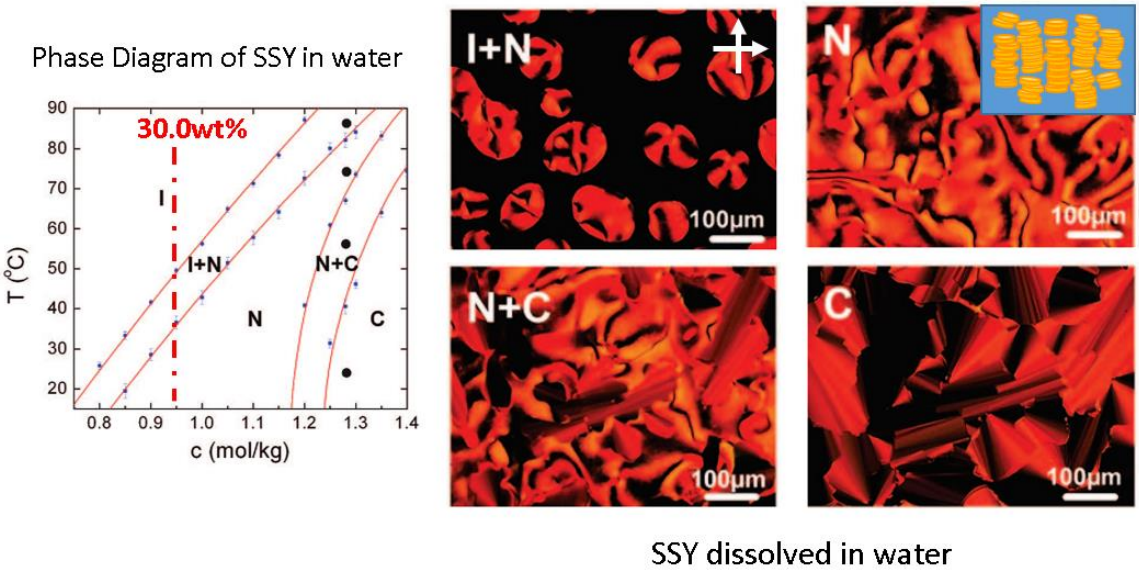

Figure 1- 3. Phase diagram of SSY in water. Experimental pictures are taken under cross-polarizers. [5] White arrows indicate the cross polarizer and analyzer. The inset is the schematic picture of the nematic phase.

1.3. Elastic Properties of LCLCs

Before introducing unique elastic properties of LCLCs [6]–[10], a director should be defined first. See the figure 1-4, the aggregates of the nematic phase are aligned along the z-direction. These aggregates' average orientational direction in local is defined as the director and it is denoted with a double arrow or a rod-like a rod in the scheme.

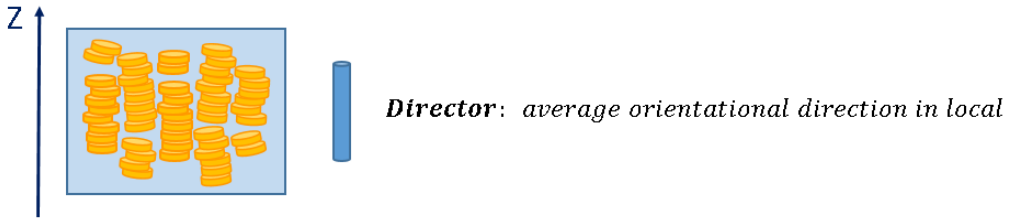

Figure 1- 4. The nematic phase scheme has an orientational order in z-direction which is denoted by the director.

It is helpful to understand the unusual elastic properties of LCLCs through Oseen-Frank Free Energy (1.1) which illustrates an energetics of confined LCLCs structure. The Oseen-Frank Free Energy is a sum of four kinds of deformations: splay (K_1), twist (K_2), bend (K_3), and saddle-splay

(K_{24}). In the energy equation, each term is a product of an intrinsic deformation constant, the elastic modulus (K), and the corresponding deformation consisting of a differential operator and a coordinate of unit director ($\hat{n}$).

Oseen-Frank Free Energy

$$\boldsymbol{F = \frac{1}{2}\int d^3x[K_1(\hat{n}\nabla\cdot\hat{n})^2 + K_2(\hat{n}\cdot\nabla\times\hat{n})^2 + K_3(\hat{n}\times\nabla\times\hat{n})^2 - K_{24}\nabla\cdot(\hat{n}\times\nabla\times\hat{n} + \hat{n}\nabla\cdot\hat{n})]}$$

(1.1)

The terms with plus are splay, twist, and bend hence these deformations increase energy. On the contrary, the minus term, saddle-splay deformation decreases energy as this deformation appears more counter-intuitively. To explain saddle-splay elasticity further, this bulk deformation term can be modified to surface deformation through a divergence theorem. For a curved surface, the saddle-splay elasticity makes the directors align along a larger principal curvature like in the figure 1-5. [11] This alignment way is reducing the total elastic free energy on the surface by the saddle-splay elasticity.

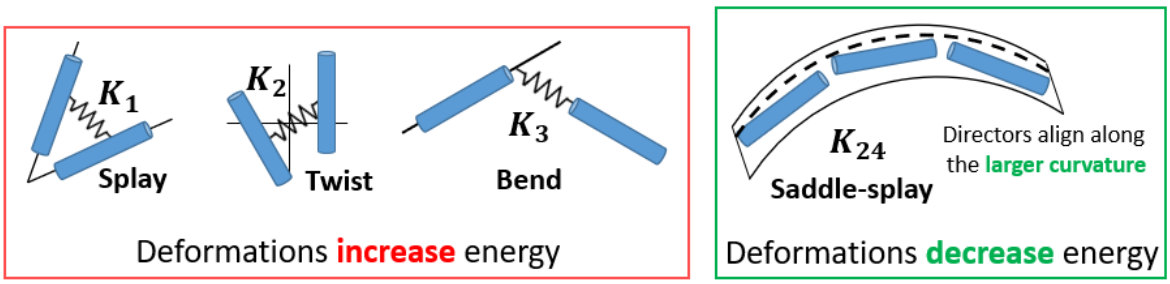

Figure 1- 5. The schematic picture for deformations: splay, twist, bend, and saddle-splay. In the case of saddle-splay elasticity, the directors align along the larger principal curvature on the surface.

Next, see the table 1-1 of comparing elastic moduli of thermotropic LC and two representative LCLCs. [7], [8], [12], [13] While all elastic moduli have the same order for the thermotropic LC, the LCLCs' twist elastic modulus is smaller by an order and the saddle-splay elastic modulus is relatively large compared to other elastic moduli. To sum up, in case of LCLCs, the twist deformation is far more preferred than splay and bend and the energy saving of the saddle-splay deformation is very large.

	K(pN) at 25℃	Splay K_1	Twist K_2	Bend K_3	Saddle-splay K_{24}
Thermotropic	5CB	6.6	3.0	10	~10
Lyotropic chromonic	Sunset Yellow (SSY, 31.5wt%)	8.4	0.8	8.1	~50
	Disodium Cromoglycate (DSCG, 14.0wt%)	8	0.6	18	13.5 ~ 31.5

Table 1- 1. Included in this table are the elastic moduli of thermotropic LC and representative LCLCs. [7,8,12,13]

The lyotropic chromonic liquid crystals are interesting matter in that they have unique anisotropic elasticity to see novel phenomenon such as chiral symmetry breaking. Also, they provide a new experimental and applicative testbed for bio-materials because of biocompatibility. [14], [15] Furthermore, LCLCs interact with water-soluble matters so they have potential benefits to be developed as a biosensor [16], for example, by using sensitivity to chiral molecules. Because of these unique properties of LCLCs mentioned, they have been actively studied nowadays and investigation on a dopant's effects on LCLCs are one of the subjects.

1.4. Previous Studies of Doped LCLCs

In figure 1-6, representative studies of doped LCLCs are presented. Since the LCLCs are water-based, the ions such as in (a) have been doped to understand mainly the aggregate behaviors, phase diagram, and LC elasticity of LCLCs. [5], [17]–[34] As seen in the figure 1-6 (b), the chiral molecules transform either left- or right- twisted structure of LCLC droplets into only one twist-handed droplets even though there is no intrinsic chirality in LCLCs. Also, the chiral dopants turn the nematic phase of LCLCs to chiral nematic phase and regarding pitch measurements have been investigated. [35]–[49] In (c), the water-soluble polymers are employed as a crowding agent in LCLCs to study the phase transition and configuration of confined LCLCs. [23], [50]–[52] Lastly in (d), it is recently studied that a surfactant doping significantly helps enhancement of LCLCs' alignment. [53], [54] In addition to that, the phase diagram is studied as a function of two kinds of LCLCs. [55] To our interest, we study the effects of a neutral polymer on the confined LCLCs and find how the dopant affects phase transition and director configuration.

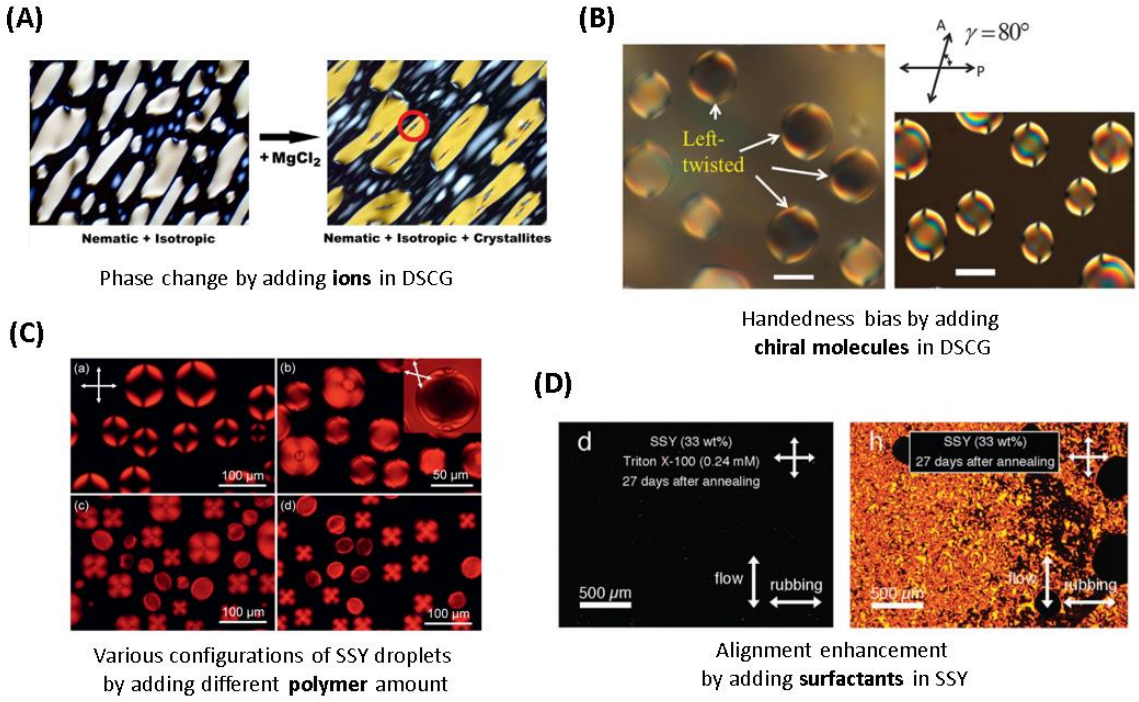

Figure 1- 6. Previous studies on doping LCLCs. (A) Added ion affects the phase of DSCG. [29] (B) The droplets of DSCG in the left picture are either left-twisted or right-twisted. [49] The chiral dopant makes the droplets have only one twist handedness in the right picture. The cross arrows indicate a polarizer (P) and an analyzer (A). Gamma is an angle between them. (C) The SSY droplets have different configurations according to the amount of the polymer doping. [52] The white arrows denote cross polarizers. (D) The two pictures are the alignment of SSY with and without the surfactant doping taken under the cross polarizers. [54] The surfactant-doped SSY aligns much better than pure SSY. The double arrow each denotes flow and rubbing directions respectively.

II Experimental Method & Materials

2.1. Sample Preparation

Sunset Yellow is purchased from Sigma Aldrich and purified following a precedent precipitation method [56] to increase the original purity of >90%. We prepare the nematic phase SSY solution by dissolving the purified SSY powder in the deionized water at a known concentration, e.g., 30.0wt%. In the same fashion, the dopant, poly(ethylene glycol) (PEG, Sigma Aldrich, average molecular weight: 35,000) is purchased and dissolved in the deionized water. All dissolved solutions in tubes are kept for minutes in an oven set as 65 Celsius degrees and mixed on a vortex rotator to be well dissolved and be uniform completely. To dope the SSY solution, we mix the SSY- and PEG- dissolved solutions properly for controlling the dopant amount at nearly fixed SSY concentration. For example, 99.6uL of 30.0wt% SSY solution and 0.4uL of 2.5wt% PEG MW 35K solution are mixed to have 0.01wt% PEG of MW 35K doped nearly 30.0wt% SSY solution. We find the PEG separates SSY into the nematic and the isotropic phase, so every sample is doped by PEG less than 0.1wt% to minimize the isotropic phase and it is safe to say that the isotropic phase is negligible. The doped SSY solution is confined to an untreated glass capillary from Vitrocom. By a capillary force, the solution fills the capillary. Then the filled capillary is put on a slide glass and glued at the ends with epoxy to be fixed and to minimize water evaporation. On the fixed capillary, another cover glass is put on and a refractive index matching oil (n = 1.474 at wavelength 589.3nm, Cargile) fills the in-between space. Before observation, we put all the samples on a temperature controller (Linkam T95-PE120) heated to the isotropic phase and cooled to the nematic phase at 21 Celsius degrees with the cooling rate from 2 to 4 K/min. Observations are conducted after 4 hours of relaxation of the samples.

2.2. Glass Coating

To attach poly(ethylene glycol) to the glass, PEG chains having silane functional group are purchased. For short PEG chains (monomers: 5), we use N-(triethoxysilylpropyl)-o-polyethylene oxide urethane, 95% from Gelest Inc. In case of long PEG chains (Molecular Weight: 2,000, 5,000, 20,000), mPEG-Silane is purchased from Laysan Bio, Inc. First, glasses (Duran group) are cleaned and surface-activated in NaOH solution at 70 Celsius degrees for 3 minutes in an oven. Then after several times of rinsing the glasses with DI water, we dip the glasses into PEG-silane dissolved toluene solution for hours. Lastly, the glasses are placed out of the solution and kept in the oven at 110 Celsius degrees for 40 minutes. As a result, PEG chains make covalent bonds with the glass via silane functional group to

coat the glass with PEG chains. For attaching much longer PEG MW 35,000, we use a two-step method to link glass and PEGs using silane medium, (3-Glycidyloxypropyl)trimethoxysilane (Sigma Aldrich). We also coat the glasses with plus charged materials, (3-Aminopropyl)triethoxysilane (APTES) and poly-lysine bought from Sigma Aldrich. Detailed coating recipes are written in the supplement.

2.3. Contact Angle Measurement

To measure the contact angle between glass and isotropic-nematic interface of the nematic droplet born in bulk, let the nematic droplets grow to touch the glass and relax enough for 20 minutes at around 45 Celsius degrees. Then take the pictures of the nematic droplets and measure the contact angle using Contact_Angle plugin of Image J.

2.4. Optical Microscopy and Characterization of Director Configuration by Jones Matrix

All the experimental pictures are taken with a color CCD (Infinity3-6UR) attached to Olympus BX-53P. An illumination source is a quasi-monochromatic LED (center wavelength = 660nm, FWHM = 25nm; LED4D067, Thorlabs). To the sample, a polarizer and an analyzer are rotated freely and a full-wave plate (optical path difference 550nm) is inserted between them for phase retardation experiments. In particular, to investigate the director configuration, the intensities of the transmitted quasi-monochromatic light are measured through a capillary's center as a function of an angle between the polarizer and the analyzer. We designate the wide rectangle with a height of 10% of the capillary diameter as the intensity measurement region. To attain intensity profiles, both the polarizer and the analyzer are parallel to the capillary axis and only the analyzer is rotated counterclockwise by 5 degrees after each intensity measurement is finished. More details are explained in the supplement.

III Wetting Behavior

3.1. Result

The first result is wetting behavior during phase transition from the isotropic to the nematic phase while temperature cools. In the figure 3-1, for the neat SSY 30.0wt% confined to the cylindrical capillary, the nematic phase nucleates at the glass wall to form the cylindrical nematic shell and it thickens as the temperature goes down. This nucleation of the nematic phase can be seen as the complete wetting on the glass with regard to wettability.

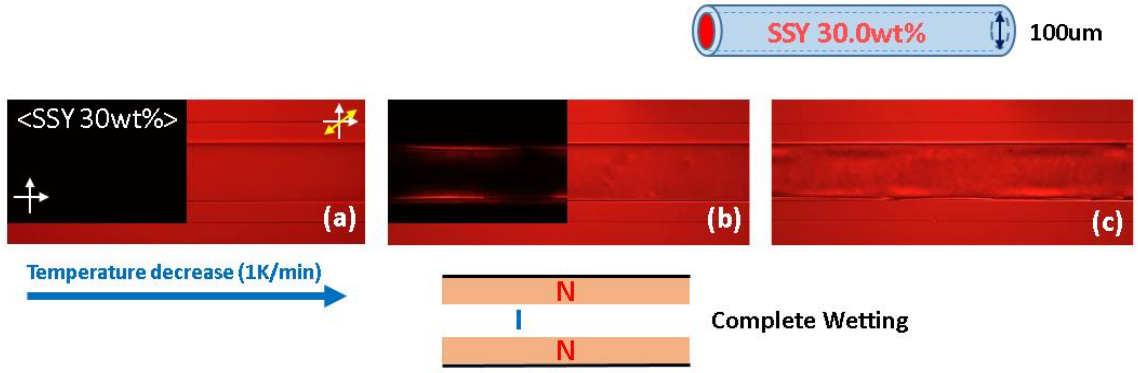

Figure 3- 1. Top scheme shows the experiment system, SSY confined to a cylindrical capillary of an inner diameter 100um. Experimental pictures are a sequence of the nematic phase nucleation during the temperature cooling at the rate of 1K/min. (a) Whole isotropic phase (b) Nematic phase starts to nucleate from the glass wall. (c) The nematic cylindrical shell thickens. The white arrows are cross polarizer and analyzer. The yellow arrow indicates a slow axis of the full-wave plate. The insets show at where the nematic phase begins to nucleate. In the full-wave plate inserted images, bright and dark jiggles show the existent nematic phase. Bottom scheme is a profile of the capillary cross section illustrating the nematic phase nucleation.

As seen in figure 3-2, despite PEG of MW 35K doping, e.g., 0.01wt%, the wetting behavior changes like that the nematic phase nucleates in bulk as droplets with no nucleation at the glass. In other words, the wetting behavior of the nematic phase changes from the complete wetting to the non-wetting on the glass.

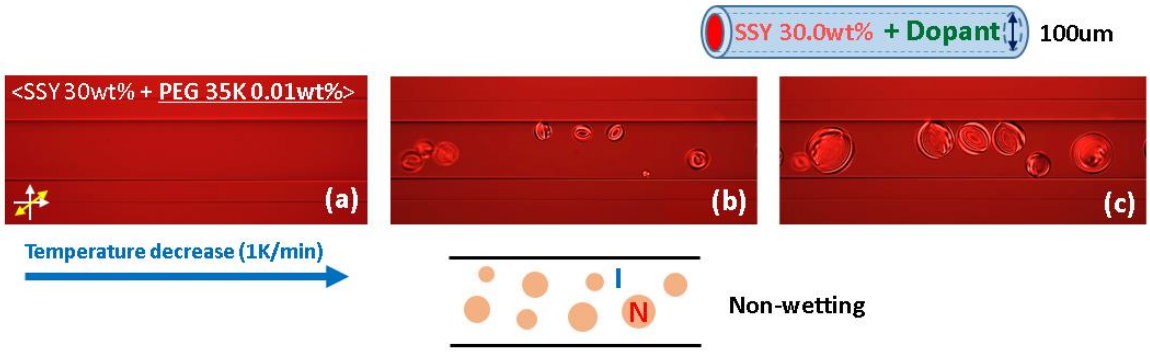

Figure 3- 2. Top scheme shows the experiment system, PEG-doped SSY confined to a cylindrical capillary of an inner diameter 100um. Experimental pictures are a sequence of the nematic phase nucleation during the temperature cooling at the rate of 1K/min. (a) Whole isotropic phase (b) Nematic phase starts to nucleate in bulk as droplets. (c) The nematic droplets grow. The white arrows are cross polarizer and analyzer. The yellow arrow indicates a slow axis of the full-wave plate. In the full-wave plate inserted images, the nematic droplets are shown having bright and dark jiggles and stripes. Bottom scheme is a profile of the capillary cross section illustrating the nematic phase nucleation.

Focusing on this intriguing wetting behavior change, we study the wetting behavior of the doped SSY nematic phase varying PEG's molecular weight and concentration as seen in the figure 3-3. The contact angle is a quantified degree of the wettability and is measured as the angle between the glass and an I-N interface when the nematic droplets nucleate in bulk and grow to touch the glass and relax enough. To illustrate the graph in the figure 3-3, for PEG of MW 35K, doping of 0.001wt% does not affect wetting behavior as the contact angle is zero so the nematic phase nucleates from the glass during the phase transition. Adding the dopant more, however, the contact angle soars from 0 to around 160 degrees indicating from the complete to the non-wetting. The dopant concentration of 0.003wt% and over, the wetting behavior is consistent like the nematic phase nucleates in bulk. Next case is PEG of MW 8K whose tendency is similar to that of PEG of MW 35K except for the smallest dopant concentration. This difference would be caused by the dissimilar spatial structure of different-MW PEGs. While even high-concentration doping of PEG of MW 400 does not change the wetting behavior up to 0.1wt% like the contact angle is fixed at zero degrees. In short, the small-MW or short-length PEG seems not to change the wetting behavior, but the large-MW or long-length PEG changes the wetting behavior considerably even with minuscule amount doping.

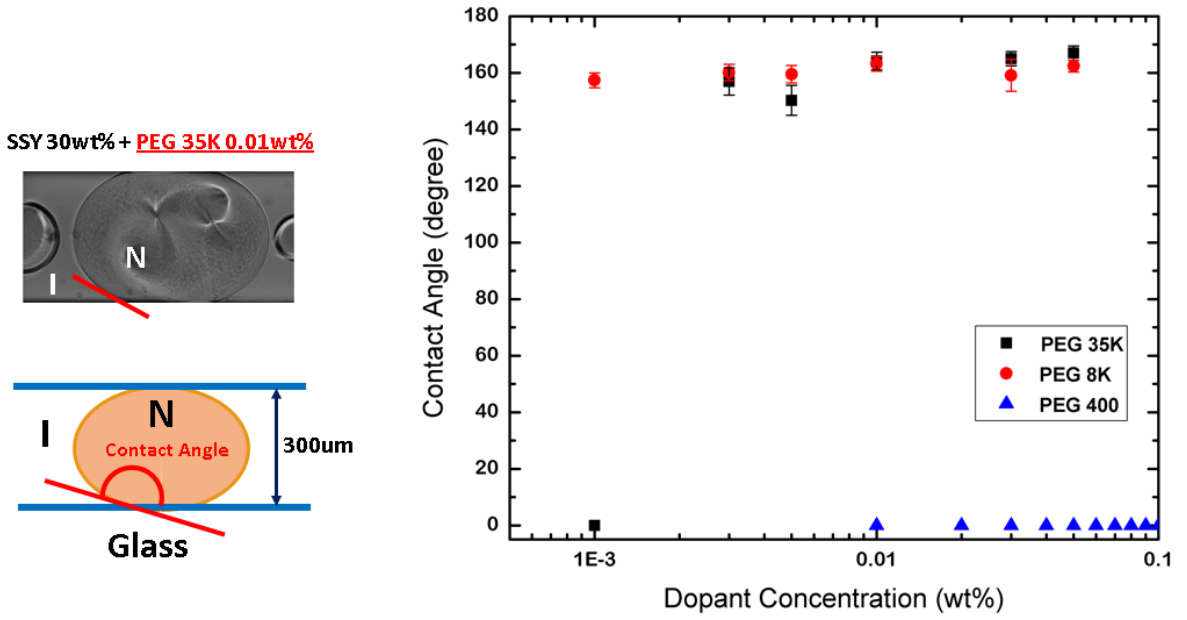

Figure 3- 3. Left-side pictures show the contact angle defined. (Top: Experiment, Bottom: Scheme) The contact angle is measured dependent on the PEG's molecular weight and concentration.

3.2. Discussion- Dopant Adsorption Model

Note the wetting difference dependent on PEG's molecular weight for the same dopant concentration so we study on what is different according to the molecular weight or the length of PEG. Hence, we find some important reference papers and introduce one of them [57] in figure 3-4. The graph from the reference shows the amount of PEG adsorption on clay minerals as a function of PEG's MW and its equilibrium concentration. In the case of PEG of MW 200, 300, and 400, the amount of adsorption on clay minerals linearly increases with the equilibrium concentration. However, for PEG of MW over 400, the adsorbed amount on clay minerals increases sharply in a regime of the equilibrium concentration below 0.15g/100ml and saturates above the concentration. Additionally, the amount of adsorbed PEG is larger as the PEG's MW is bigger for the same equilibrium concentration. Based on these points, we find a few hints on how PEG affects the wetting behavior of the nematic phase during the phase transition. First, the sharp then plateauing shape of adsorption amount of the longer PEGs is like that of the contact angle in the figure 3-3. Second, the longer PEGs adsorb more on the substrate than the shorter ones for the same equilibrium concentration. On account of these two points, we make a hypothesis that the longer (the larger MW) PEGs are better to adsorb on the glass than the shorter ones do for the same concentration in the solution and the adsorbed PEGs hinder the nematic phase from nucleating at the glass.

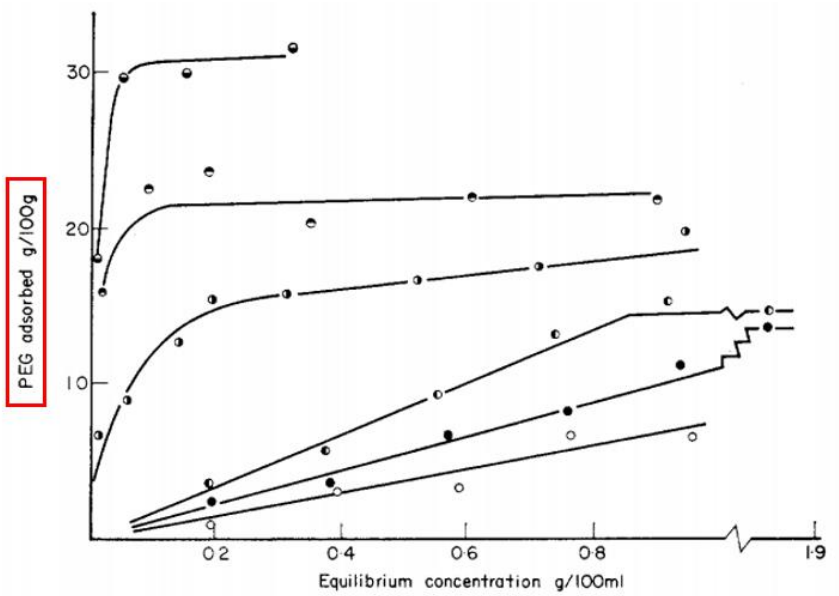

FIG. 2. Isotherms for the adsorption of PEG 200, ○, PEG 300, ●, PEG 400, ◐, PEG 600, ◑, PEG 1500, ◓, and PEG 20000, ◒, on Ca montmorillonite at 25°C.

PEG	Weight of PEG adsorbed g/100g
200	7·0
300	13·5
400	14·6
600	19·0
1500	22·2
20000	39·0

Figure 3- 4. Graph of PEG adsorbed amount on the substrate versus PEG solution concentration. [57] Right-side table indicates that the longer PEG length is, the better it adsorbs on the substrate.

In order to prove our hypothesis, we coat the glass with PEGs by making covalent bonds between PEGs and the glass via a silane functional group. Due to a wet-dry repeating coating process written in the supplement, we coat PEGs on the slide glasses instead of the inner glass of the capillary and confine the pure SSY between coated slide glasses to test our model. To see the apparent difference, we compare two cases: PEG doped SSY confined to bare glasses and neat SSY confined to a PEG-coated glass cell. In both, SSY concentration is 30.0wt% and PEG lengths are similar in that doped PEG's length is 9 and coated PEG's length is 5 monomers long. The experimental results are shown in the figure 3-5 that the nucleation of the nematic phase occurs in the sandwich cell during temperature cooling from the isotropic phase. For monomer-5 (MW 220) PEG-coated sandwich cell case in the figure 3-5 (a), the nematic phase does not nucleate on the glass, instead, it nucleates in bulk like doping MW 35K PEG 0.01wt% to SSY in the glass capillary. In the same way, we check further that the nematic phase nucleates in bulk when confined to MW-2K,5K,20K,35K PEG-coated cells. To make sure, compare the sample of monomer-9 (MW 400) PEG 0.1wt% doped to SSY in the bare glass cell. In this case, the nematic phase nucleates on the glass in the figure 3-5 (b).

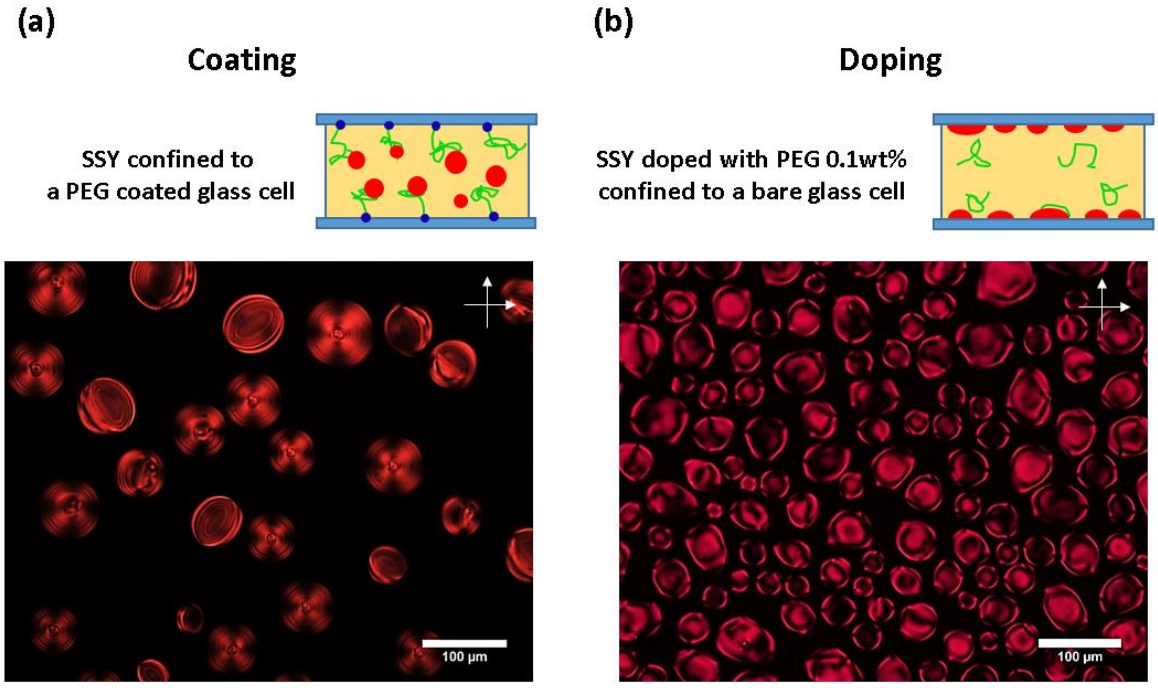

Figure 3- 5. In both (a) and (b), a sandwich cell scheme is drawn. In the schemes, color has a meaning: light blue – glass, green – PEG, yellow – isotropic phase, red – nematic phase. The blue dot is a covalent bonding between the glass and PEG in (a). Both experimental pictures are taken during the phase transition from the isotropic to the nematic phase. In (a), the nematic phase nucleates in bulk as a droplet like in the figure 3-2. The nematic phase nucleates on the glass in (b). The white arrows denote the cross polarizers.

In table 3-1, the results are organized. Note the coating section, it seems that the PEGs attached on the glass prevents the nematic phase from nucleating on the glass regardless of the length of PEG. Speaking of the length of PEG for coating, the minimum number of the monomer is 5 and the maximum is 800. The difference of the lengths is large, but seemingly the effects on the nucleation of the nematic phase are similar. Next, see the doping section saying that the longer PEG doping to SSY confined in the bare glass let the nematic phase grow in bulk, yet the smaller PEG has no effect on the nucleation even for the high amount of doping. This consequence is consistent with our PEG adsorption model that the longer PEG is, the better it adsorbs on the glass.

	Doping	Coating
Short PEG	complete wetting	Non-wetting
Long PEG	Non-wetting	Non-wetting

Table 3- 1. The table shows what condition affects the wetting behavior.

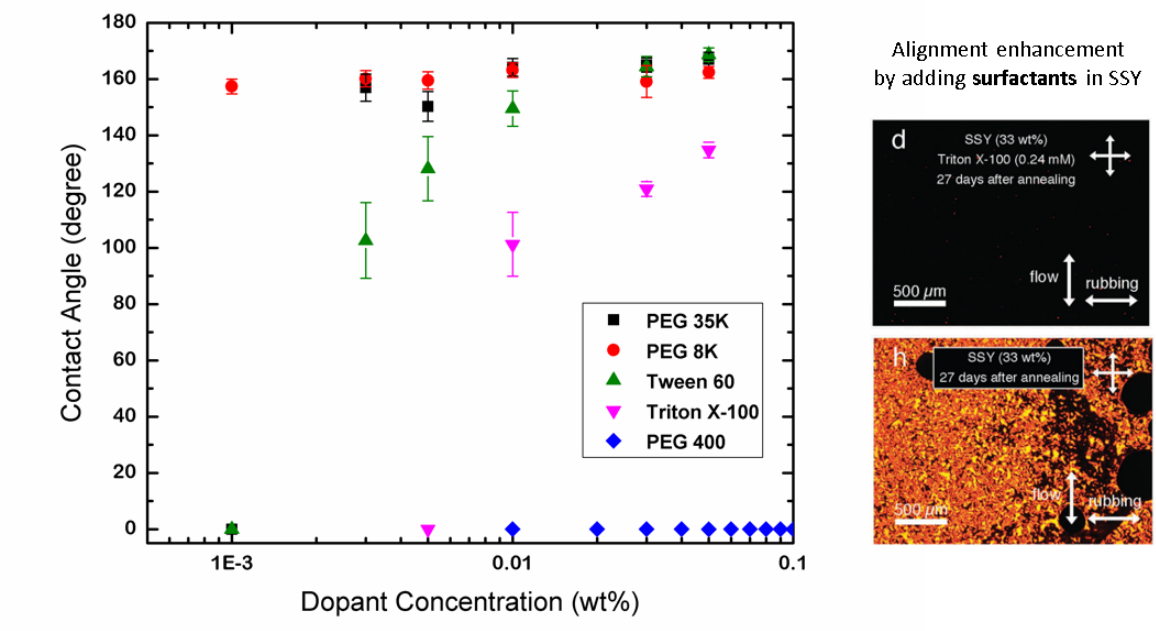

Figure 3- 6. In the graph, all dopant cases are included with PEG chain having surfactants. The surfactants show intermediate wetting tendency compared to PEGs. Right-side experimental results from reference [54] show that the surfactant Triton X-100 doping enhances the alignment of SSY in spite of minute amount doping.

In bio-field, PEG is used as a blocking agent for a protein's non-specific adsorption. Thus, we think that adsorbed PEG in our experiments plays a similar role in blocking the nucleation of the nematic phase on the glass. As seen in the figure 3-6, we continue the experiments about the wetting behavior with the surfactants having PEG chain and observe that they show intermediate wetting tendency close to PEG MW 35K but rather less sharp. With regard to the surfactant adsorption, it has been proved that minuscule Triton X-100 doping to SSY enables the alignment of SSY more stable for a long time. [54] Hence, we expect that our study on PEG adsorption will be beneficial to the alignment issue of LCLCs.

3.3. Summary of Wetting Behavior

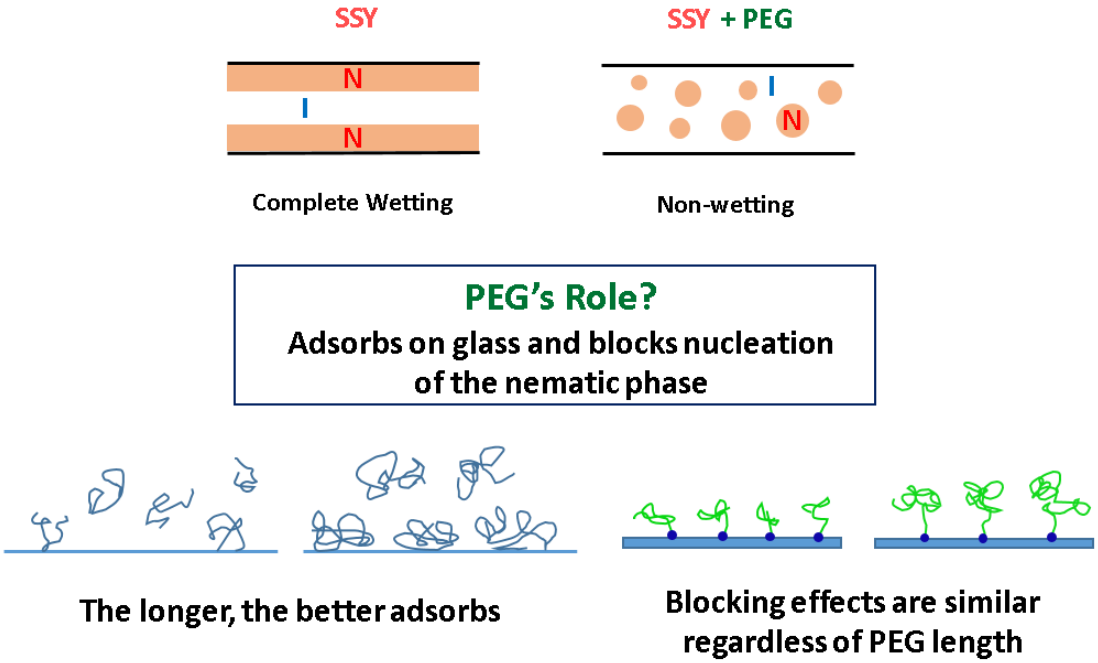

Figure 3- 7. Summary of wetting behavior.

To recapitulate the wetting behavior of SSY in the figure 3-7, the nematic nucleation starts at the glass when confined to the glass, which is the complete wetting. With minute amount of PEG MW 35K doping to SSY, however, the nematic phase nucleates in bulk, which is so-called non-wetting. This dissimilar wetting behavior is because adsorbed PEG seems to block the nucleation of the nematic phase at the glass. The adsorption of PEG is dependent on its length or molecular weight and concentration. From our adsorption model, it is partially testified that the longer PEG is, the better it adsorbs on the glass. Additionally, PEG's blocking effects to the nematic phase have nothing to do with the length of PEG once any PEG adsorbs on the glass enough.

IV Director Configuration of Confined Doped LCLCs

4.1. Result

The second result of confined PEG-doped SSY is the director configuration after the isotropic phase totally transforms into the nematic phase and the nematic phase relaxes enough to form a structure. What if SSY is confined to the cylindrical capillary then what structure would it make? From an energy perspective, minimizing deformation is preferable so it seems that all directors

should align parallel to the capillary axis to make no deformation. However, for the curved surface, LCLCs' saddle-splay elasticity becomes effective to reduce the total free energy. Near the surface, the directors align along the larger principal curvature due to the saddle-splay elastic modulus to save energy. The directors in the center prefer to align along the axis of the capillary so the directors between the axis and surface have to twist. Though the saddle-splay elasticity prefers to align near-surface directors along the larger curvature, the directors are tilted a little to the desired direction owing to the twist deformations in bulk. As a result, LCLCs happen to have a double-twist structure as seen in the figure 4-1. From the figure 4-1, you see the structure is twisted in both radial and axial directions, so-called literally double-twist. [11], [13] The DT scheme is drawn and an angle β_1 is defined, the angle between the directors at the axis and near the surface. See the whole scheme of this profile. This twist domain is left-handed and the right-handed domain is also possible due to the same energy cost, which is chiral symmetry breaking.

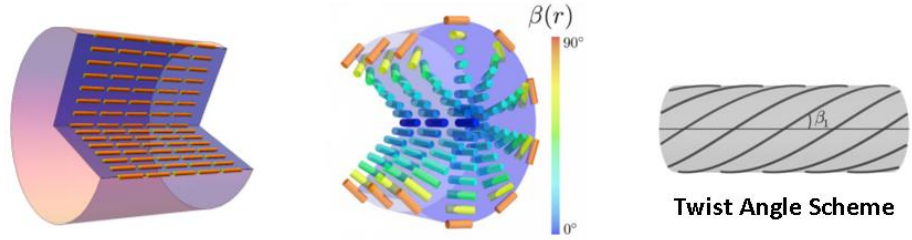

$$F = \frac{1}{2}\int d^3x[K_1(\hat{n}\nabla\cdot\hat{n})^2 + K_2(\hat{n}\cdot\nabla\times\hat{n})^2 + K_3(\hat{n}\times\nabla\times\hat{n})^2 - K_{24}\nabla\cdot(\hat{n}\times\nabla\times\hat{n} + \hat{n}\nabla\cdot\hat{n})]$$

$$K_2 \ll K_1 \approx K_3\ (pN)$$
$$K_2 \ll K_{24}\ (pN)$$

Figure 4- 1. Director configuration of parallel-axial and double-twist structures. [11] The rod denotes a director. In the DT structure, the color of the rod indicates the degree of twist to the axis. The black streamlines in the twist angle scheme are the directors on the surface in DT structure. [11] The twist angle β_1 is defined as the angle between the axis and the director on the surface. The unique elastic properties are revisited to understand why the double-twist configuration is the ground state for LCLCs under a cylinder confinement.

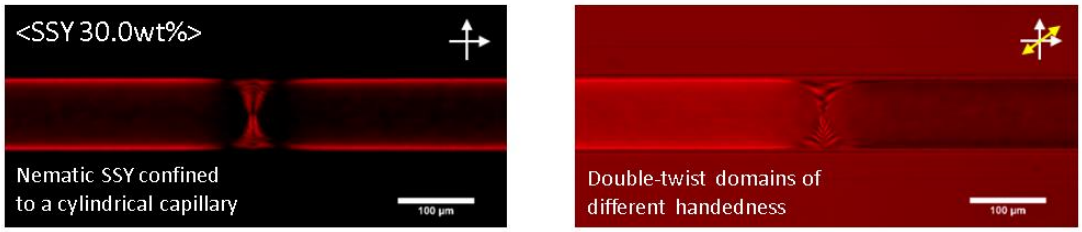

Figure 4- 2. Experimental pictures of SSY 30.0wt% confined to a cylindrical capillary. The cross white arrows are the polarizer and the analyzer. The slow axis of the full-wave plate is denoted by a yellow arrow. The two different DT domains are distinguished in the full-wave plate inserted image. Between the domains of different handedness, the point defect exists.

The experimental pictures of SSY confined to the cylindrical capillary are in the figure 4-2 and two different domains are definitely distinguished in a full-wave plate inserted picture. Here the interesting point is that the chiral symmetry breaks when LCLCs are confined to the curved surface, in spite of SSY's achiral molecular structure. In-between two dissimilar domains, a defect should be formed and is a point defect. Note that only point defects are formed for SSY confined to the cylinder cavity. [11] In the figure 4-3, here is the director configuration of PEG MW 35K doped SSY in the cylindrical confinement. The structure basically is the double-twist, but there are some changes. The first change is the appearance of several stripes in the middle of the capillary indicating that the twist angle β_1 changes from nearly 90 degrees. The second difference is a formation of an unprecedented domain wall-like defect which is never seen in pure SSY confined case.

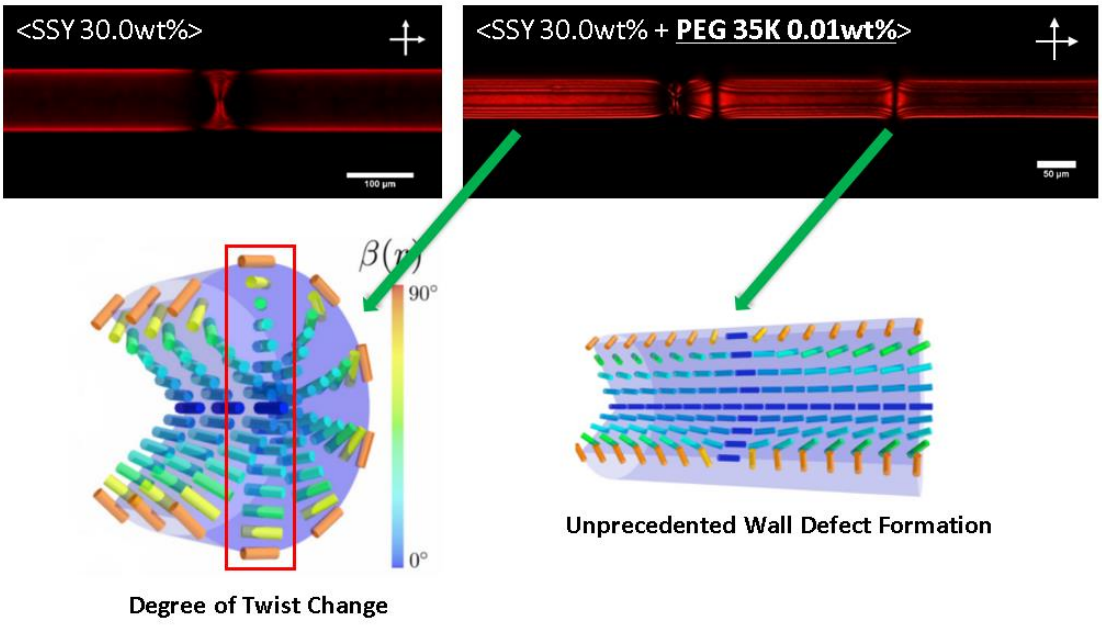

Figure 4- 3. Comparison of PEG-doped SSY confined configuration to neat SSY case. The minuscule amount of the PEG 35K affects the DT structure in two points. The first is the degree of a twist as seen in the middle of the capillary appearing stripes. The second is the formation of an unprecedented domain wall-like defect. [11]

To investigate this changed double-twist structure, we estimate the twist angle β_1 of the samples according to our method written in the supplement. In the figure 4-4, the twist angle β_1 is estimated dependent on the dopant PEG of MW 35K concentration and the capillary size. In case of an 100um size, the confined neat SSY's twist angle is close to 90 degrees. Surprisingly, the twist angle plummets down to roughly 20 degrees despite of 0.01 and 0.02wt% doping. For a 50um sized confinement, the pure SSY's twist angle is similar to that of an 100um one. However, we find the contact angle diverges into two values with doping 0.01wt% and converges to near 20 degrees with doping twice. Though there is the case which the decreased twist angles are inconsistent, the common point is that the twist angles decline. The balance between saddle-splay elasticity and twist deformation in bulk is a drive of the double-twist. In light of this, we can understand that the loose double-twist with decreased twist angle may be induced by the decreased saddle-splay elastic modulus.

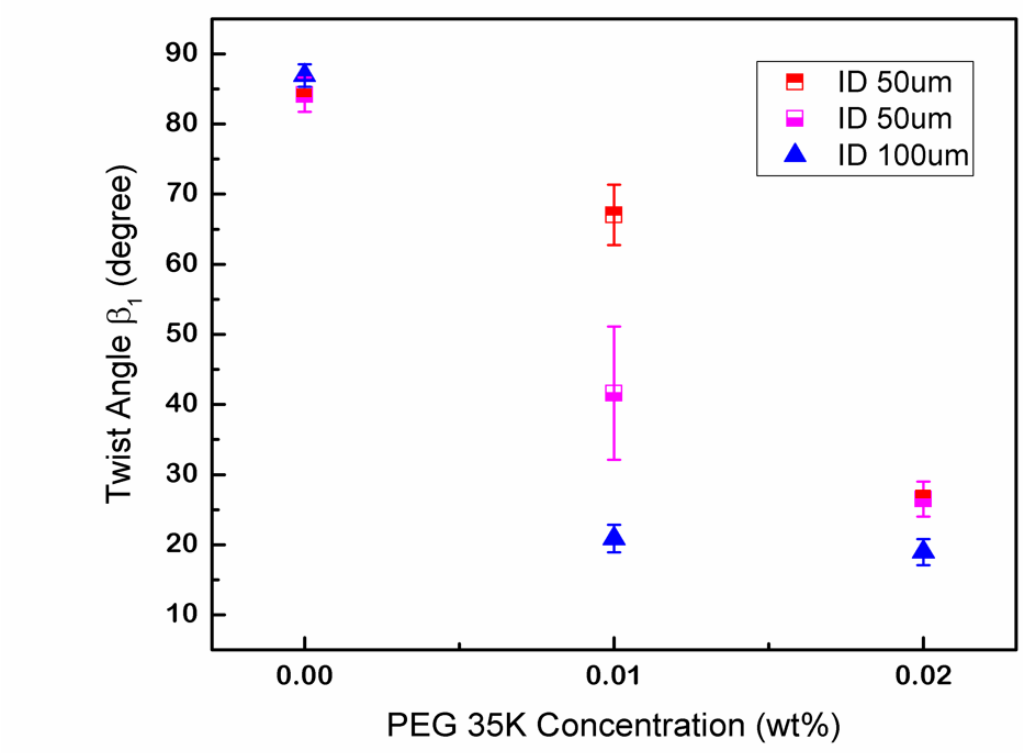

Figure 4- 4. Twist angle $\boldsymbol{\beta_1}$ of PEG-doped SSY's double-twist is drawn dependent on the concentration of PEG and the size of the confining cylinder. The twist angle diverges only for PEG 0.01wt% doped case confined to an ID 50um cylinder shown in half hollow squares. Filled squares indicate the twist angle has a single value.

Next comparison of pure and doped SSY configurations is under a square capillary having round corners as seen from the cross-section in the figure 4-5. Because of these round corners, the saddle-splay elasticity comes into play so the pure SSY forms the double-twist and has a point defect just like when confined in the cylindrical capillary. [10] However, adding the minuscule

amount of PEG to SSY, the SSY in the square confinement has a long-ranged parallel-axial alignment with intermittent defects. In the same context as the cylinder confinement above, we understand the emergence of parallel-axial alignment with a decreased elastic modulus of saddle-splay. If it decreases, energy saving effect also diminishes which originally offsets the twist deformation in bulk and the total energy increases beyond the energy of forming parallel-axial alignment. In consequence, the parallel-axial alignment is favored over the double-twist.

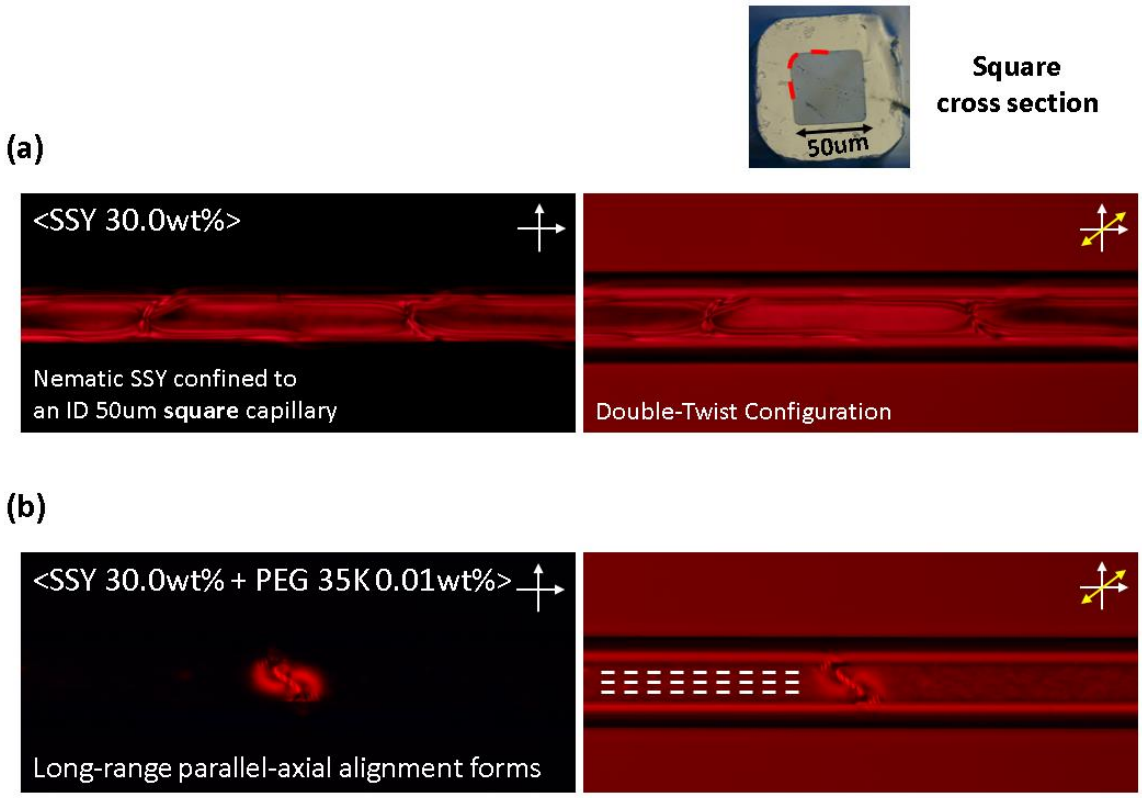

Figure 4- 5 SSY and PEG-doped SSY confined to a square capillary. (a) Double-twist configuration with point defects, (b) Parallel-axial configuration with a defect. In the square's cross-section, the red dotted line shows the square capillary has round corners which make the saddle-splay elasticity effective. The cross polarizer and analyzer are drawn as white arrows. The full-wave plate's slow axis is denoted by a yellow arrow. In the full-wave plate inserted image of (b), the little white lines indicate the directors of parallel-axial configuration.

To summarize, the minute amount of PEG doping induces the twist angle decrease and the domain-wall like defect formation in the double-twist structure of neat SSY confined to the cylinder cavity. Besides, the doping allows the SSY to have the long-ranged parallel-axial alignment in the square confinement. Particularly decreased saddle-splay elastic modulus would make the twist angle decrease of the double-twist structure in the cylinder and the parallel-axial alignment in the square. Therefore, we investigate whether the saddle-splay elastic modulus is reduced by the minute amount of PEG.

4.2. Discussion- Metastable State

The SSY's double-twist configuration is characterized in the reference so we take the well-illustrated graph in terms of elastic moduli and energy. [11] Specifically, in figure 4-6, the y-axis is the energy difference between the double-twist with a defect and without a defect. There are two kinds of defects: a point and a domain-wall like defects. In the graph, corresponding defect energy lines are drawn. Note that here K means both splay and bend elastic moduli but is used to denote bend only due to none of the play deformation in the double-twist. The bottom x-axis is a ratio of saddle-splay elastic modulus over bend one, K_24 / K. The twist angle set as a top x-axis has a relationship with K_24 / K as seen in the equation (4.1). [11]

$$\boldsymbol{\beta_1 = arctan\sqrt{\frac{K\_24/K(K_{24}-2K_2)}{K_2}}} \qquad (4.1.)$$

In the figure 4-6 (a), the calculations are done with fixing K_2 / K as 1/10. Follow the red arrow. Without the dopant, the twist angle is around 87 degrees and making a point defect is preferable in light of energy. It is also consistent with the experiments. However, doping makes the twist angle diminish to 20 to 60 degrees, which means the saddle-splay elastic modulus decreases even to a few tenths of it. Also, only domain wall-like defects should be formed but the point defects always outnumber their counterparts in the experiments. On account of this, it is implausible that minuscule amount of the dopant reduces saddle-splay elastic modulus largely so we try other calculations opening up for the dopant's effects on other elastic modulus, e.g. twist, as well as saddle-splay one. In the figure 4-6 (b), K_2 increases 5 times so K_2 / K as 1/2 is fixed. In the graph (b), K_24 should diminish more than 3 times to have such decreased twist angle. This time the energy gap between the formation of two defects narrows yet point defect's outnumbering is unraveled. Still, such a tiny amount of PEG's effects on a drastic change of elastic moduli raise a question so we focus on other nontrivial aspects of this phenomenon.

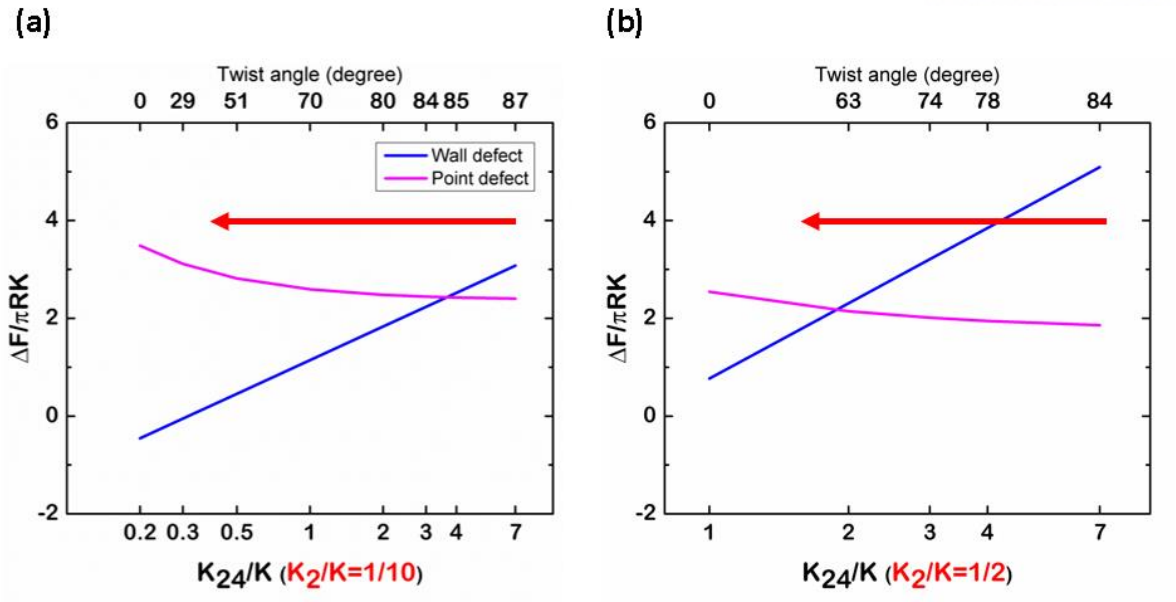

Figure 4- 6. Relative energy cost of forming a point and a domain-wall like defects as a function of either **K_24/K** or equivalent twist angle. [11] The y-axis is the energy difference of double-twist with and without a defect. The bottom x-axis is the ratio of saddle-splay elastic modulus over bend one and the x-axes are correlated with the equation (4.1). The twist to bed ratio in parenthesis is fixed value to calculate the energy. The red arrow in (a), (b) denote the twist angle decrease by doping. F: Oseen-Frank energy, R: radius of the capillary, K: splay and bend elastic moduli

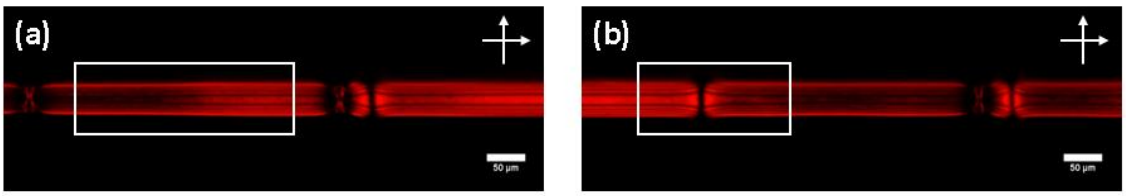

Figure 4- 7. The samples of PEG of MW 35K 0.01wt% doped to SSY confined to an ID 50um cylindrical capillary. In the white boxes, the heterogeneity of the twist angle is shown. (a) The twist angle changes over the same domain. (b) The defect's left- and right- side domains have different twist angles. The white arrows denote the cross-polarizer and analyzer.

Firstly, the twist angles are not homogeneous for the same dopant's concentration as previously seen in the figure 4-4. Except for PEG 0.01wt% of MW 35K doped to SSY in ID 50um confinement, it seems that the twist angle is consistent but every PEG-doped sample has heterogeneous twist angle distribution just like in the figure 4-7. In the single domain of the sample in the white box in (a), the twist angle varies along the horizontal direction as seen in the appearance of the red stripes. In addition, the domains of having different twist angles form the defect denoted by the white box in (b). Secondly, a number ratio of two kinds of defects is arbitrary for any dopant concentration. As mentioned earlier, the point defects outnumber always the domain-

wall like defects. Besides, the number portion of these two defects differs each time after going through heat-cool cycles. This point casts doubt on an equilibrium state of the samples because the number ratio of the defects should be consistent following Boltzmann distribution if the state is in the equilibrium. Lastly, it is believed that the dopant PEG adsorbs on the glass wall and affects basically the way the nematic phase nucleates. These three points lead us to conclude that the confined PEG-doped SSY is in the metastable state in which the sample's system remains semi-permanently because of failing to overcome high energy barrier for going in the equilibrium state.

4.3. Summary of Director Configuration of Confined Doped LCLCs

To summarize the second result of confined doped LCLCs, the addition of PEG has the double-twist of SSY be the metastable state. Even though the PEG on SSY's double-twist induces the twist angle decrease and the domain-wall like defect formation, corresponding energy characterization tells us that the amount of the dopant is too small to affect significant changes in elastic moduli, e.g., saddle-splay elastic modulus. Besides, the twist angle distributes inconsistently and heterogeneously through the domains of the double-twist and the defects' number ratio is arbitrary against Boltzmann distribution. Moreover, the different way of nucleation of the nematic phase is non-negligible. In conclusion, the confined PEG-doped LCLCs make metastable double-twist configurations with unprecedented characteristics.

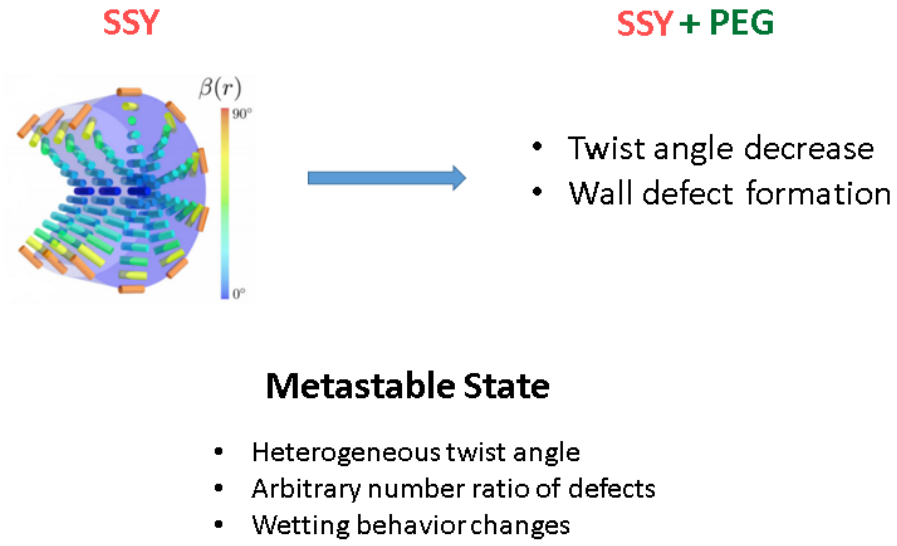

Figure 4- 8. Summary of the director configuration state of confined PEG doped LCLCs [11]

V Summary & Conclusion

We study the neutral polymer PEG's effects on confined LCLCs with respect to wetting behavior and director configuration. The nucleation of the nematic phase starts at the glass during the phase transition from the isotropic phase when the pure SSY is confined to a glass capillary. Specifically, the nematic phase nucleates on the whole glass to form the nematic shell, which is the nematic phase's complete wetting on the glass. On the contrary, the PEG of MW 35K-doped SSY does not nucleate on the glass instead of in bulk as droplets despite the minute amount of the dopant. The dopant PEG changes the site of nucleation of the nematic phase or the wetting behavior from complete to non-wetting. The cylinder-confined SSY forms the DT configuration with and without the dopant addition as a result of the phase transition from the isotropic phase to the nematic phase. Yet, the dopant PEG affects the DT configuration to have decreased twist angle and an unprecedented kind of defect. Due to these results, we expect that saddle-splay elastic modulus and others would be changed but this significant change seems improbable considering the minuscule amount doping. Thus, we conclude that the dopant addition leads the DT structure to a metastable state having heterogeneous twist angle distribution and the arbitrary number ratio of two kinds of defects. Lastly, we consider the changed wetting dynamics strongly affects to form the metastable states.

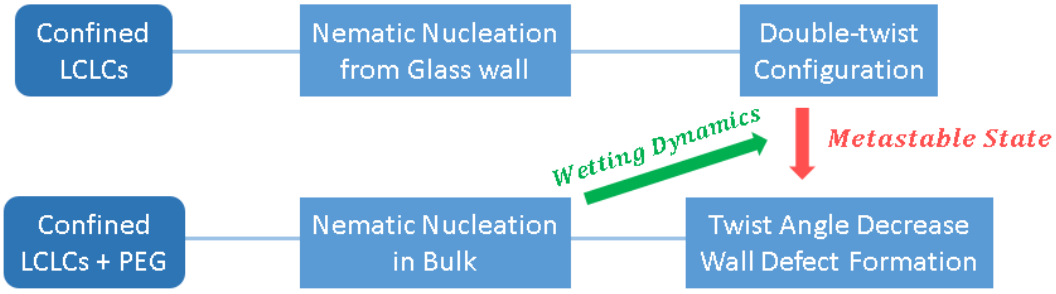

Figure 5- 1. Overall summary of the paper.

VI Supplementary Information

6.1. Coating Recipes

Here is the list of coating materials:
PEG of monomer 5 - N-(triethoxysilylpropyl)-o-polyethylene oxide urethane, 95% (silane) from Gelest Inc.
PEG of MW 2,000, 5,000, 20,000 - mPEG-Silane from Laysan Bio, Inc.
PEG of MW 35,000 powder - (3-Glycidyloxypropyl)trimethoxysilane (silane medium) from Sigma Aldrich
Plus charged materials - (3-Aminopropyl)triethoxysilane (APTES) and poly-lysine from Sigma Aldrich

Materials with the silane functional group coating recipes include reagents preparation, cleaning and surface activation, cleaning and drying, reaction, baking, cleaning and drying, and management. We name this coating procedure as the silane coating method.

The silane coating method applies to PEG of monomer 5, mPEG-Silane, APTES (only difference in the reagent), and partially to PEG of MW 35K (to connect silane medium to glass).

Here follows **<Silane Coating Method>**. The lines in the curved parenthesis are cautions.

1. Reagents preparation

Make a 10wt% NaOH aqueous solution.
{APTES forms polymers when in contact with moisture. It is recommended all the solutions (reagents) are made in the hood as it is fully filled with the nitrogen gas.}

Prepare the glass bottle with its cap and magnetic stirrer each for each reagent.
Make the 10mM solution with the solvent toluene depending on what to coat, PEG or APTES.
-10mM PEG-Silane solution= toluene 200mL + PEG-Silane 1000uL
-10mM APTES solution= toluene 200mL + APTES 500uL

Keep the solutions stirred with the magnet at least 1 hour.
{You can reuse reagent solution 8 times at maximum.}

2. Cleaning and surface activation

Clean the holders with detergent and wash them with acetone.
If any slide glass or cover slip is greasy, wash it with acetone first, then with DI water and dry it thoroughly.
Fill each holder with slide glasses and cover slips.
{Before reaction is finished, you should not touch the holder body to prevent any contamination. Grab the handles of the holders.}

Pour NaOH 10wt% solution in a P.P. or Teflon container to the extent of dipping the holder body.
Then put the container filled with the solution in the 70C oven and wait for enough till the solution is heated to 70C.

After sufficient time, dip the holders into the container for 3 minutes inside the oven. You are making the glass surface activated by attaching hydroxyl ions to it. You can check this easily from the wetting angle of water droplets.

3. Cleaning and Drying

After 3 minutes in the oven, take the holders out from the container and dip into the DI water. Sonicate the holders in the DI water for 3 to 5 minutes. Then dip them into the fresh DI water and wash them 7 times more.
{Drying should be done right before reaction. Before reaction, just leave the glasses dipped into the DI water.}

Dry the glasses, coverslips, and holders thoroughly by nitrogen gas gun in the extent to that no water remains seemingly. You should clean the desiccator and check the vacuum function before drying. Then put them in a desiccator for 15~20 minutes. (This process is optimized to remain very thin layer of water.)

4. Reaction (making hydrogen bonds)

Because the reagents are susceptible to the moisture, it is desirable that the reaction is done in the hood filled with the nitrogen gas. Prepare the small, big containers, and big container cover.
Put the small container in the big container and pour the reagent solution (APTES or PEG-Silane) into the small container.

Dip the holders in the solution and cover the small container and the holder with aluminum foil to prevent toluene melting the plastic cover.
Lastly, cover totally the big container with its cover to prevent any moisture.
You should keep them at least 2 hours but it is okay as long as the holders are in the solution. In other words, you can preserve them in the solution for a long time.

5. Baking (forming covalent bonds)

After two hours, pull the holders out, dip into fresh toluene for a moment, and dry thoroughly by nitrogen gas gun in a previous way.
Bake the holders in the 110C oven for 40 minutes (80C 1hour).
After 40 minutes, cool the holders to the room temperature.

6. Cleaning and drying

Wash the holders with ethanol and sonicate them in the ethanol for 3 minutes 3 times. After sonication, wash again them with the ethanol.
Dry them thoroughly with the nitrogen gas and put them in the desiccator for 15~20 minutes.

7. Management

Store the coated glasses and coverslips in a box and seal it thoroughly. You can use them up to one year. All the solution should be discarded into an organic solvent.
Any containers contacted with the reagents should be washed with ethanol first then with the detergent.

To coat PEG of MW 35K powders, similar steps are followed with different reagents.

Dissolve PEG 35K powders of 40g into dichloromethane of 400mL and add sulfuric acid of 20uL as a catalyst.
After completely dissolving the reagent solution, dip the silane-coated glasses into this solution and keep it at least 10 hours. (The duration time is not optimized so the proper time should be found through further try and errors.)
You should cover the reaction container with its top because of low-boiling dichloromethane.

After the reaction, rinse the glasses with dichloromethane and sonicate them for 5 minutes. Lastly, wash them with ethanol and sonicate them also.
Dry them with the nitrogen gun and desiccate them in the desiccator for 15 minutes.
Store them in the same way for PEG-coated ones.

<Poly-lysine coating method>

Make a 10wt% NaOH aqueous solution and follow the silane coating method up to 3.
Then the glasses are ready for the reaction.
Paint the glasses with poly-lysine as received and keep them for 15 minutes.
It is convenient to use a petri dish, a disposable pipette, and a diamond pen to mark. The poly-lysine solution is reusable.
For cleaning, rinse them with DI water and dry them by the nitrogen gas gun.
Store them following management step.

In case of any coating, surface characterization is necessary for consistent coating and reproducible experiments. Contact angle measurement and x-ray photoelectron spectroscopy (XPS) analysis are representative characterization methods. For instance, the graphs in the figure S1 are the XPS result of PEG of MW 35K coated glass. We can check that the PEGs are well coated to the glass from the figure S1.

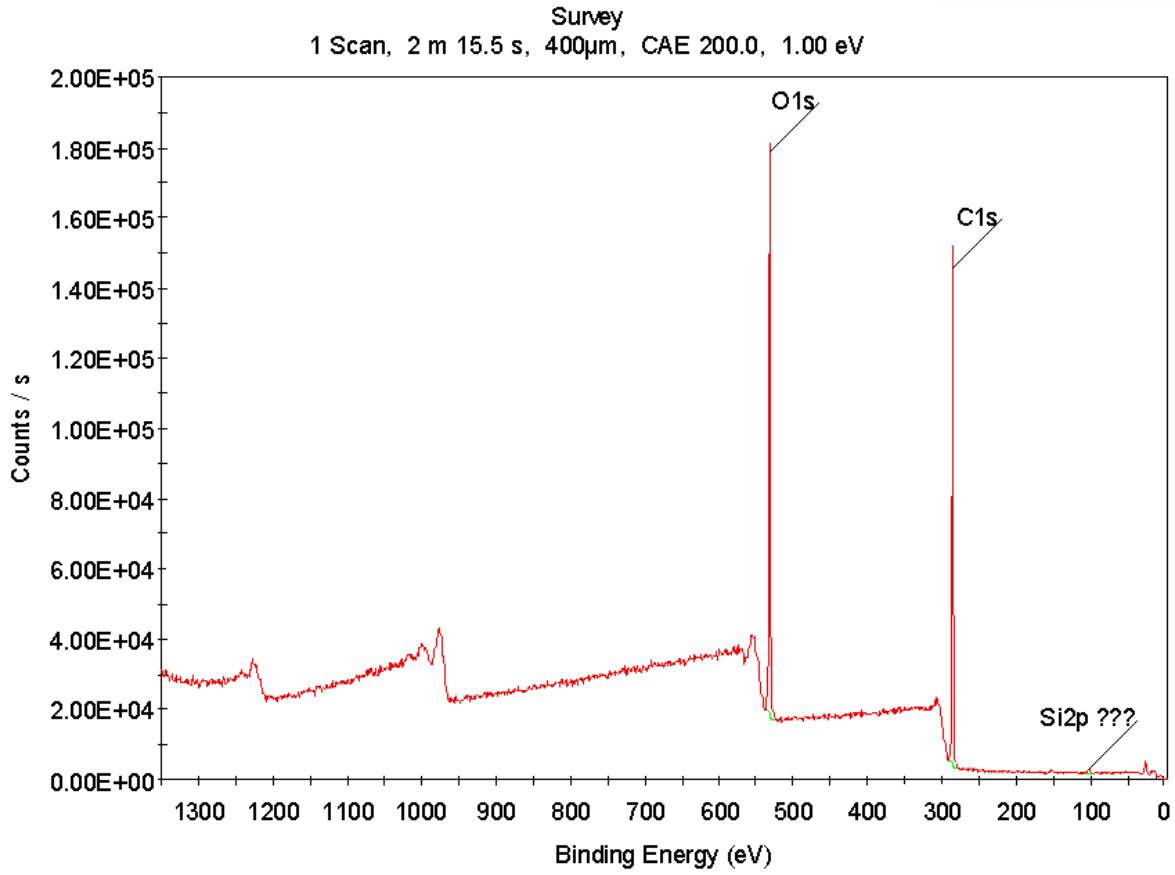

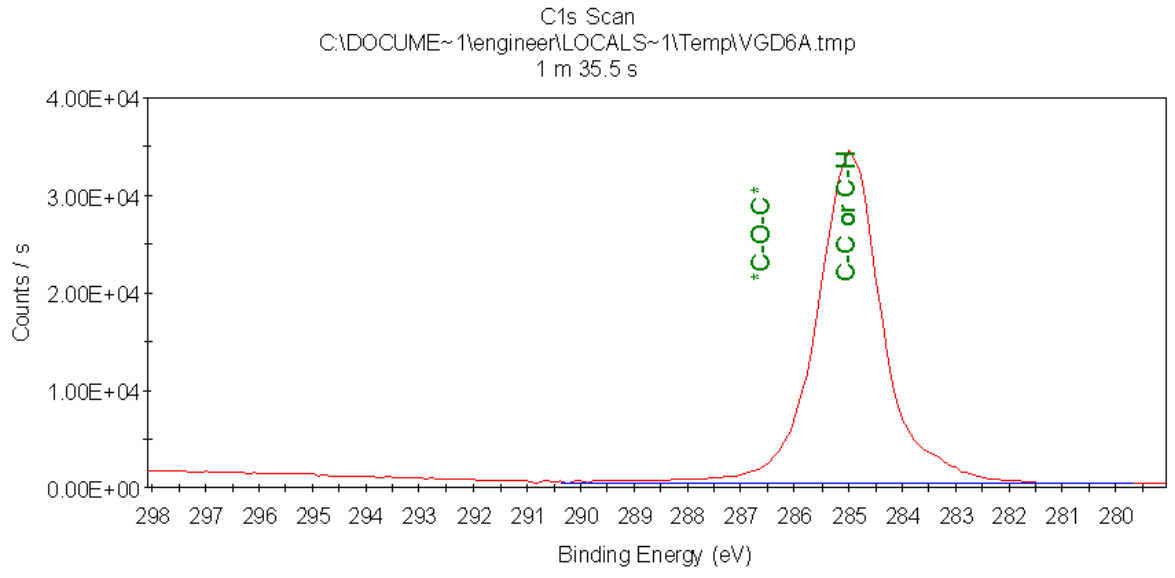

Figure S1. XPS result of PEG of MW 35K coated glass. The peaks in the first graph indicates the existence of oxygen and carbon onto the glass. From the second graph, it is found that those oxygen and carbon are from the PEG chains as seen in a broad peak which is a magnification of the second peak from the first graph.

6.2. Twist Angle Estimation Procedures with Mathematica Codes

Here are the steps of estimation of the twist angle:

1. Get an intensity profile of the (PEG-doped) SSY confined to a cylinder cavity as a function of an angle between a polarizer and an analyzer.
2. The intensity profile is compared to a numerically generated profiles of the DT configuration varying an optical birefringence and a twist angle, conducted with **code 1**.
3. Find the best matching profile by the least squared method then take the profile's parameters: the optical birefringence and the twist angle.
4. To confirm multiple parameter sets, compare the experimental polarized optical microscopy image with the 2D optical texture simulated by Jones Matrix, conducted with **code 2**.

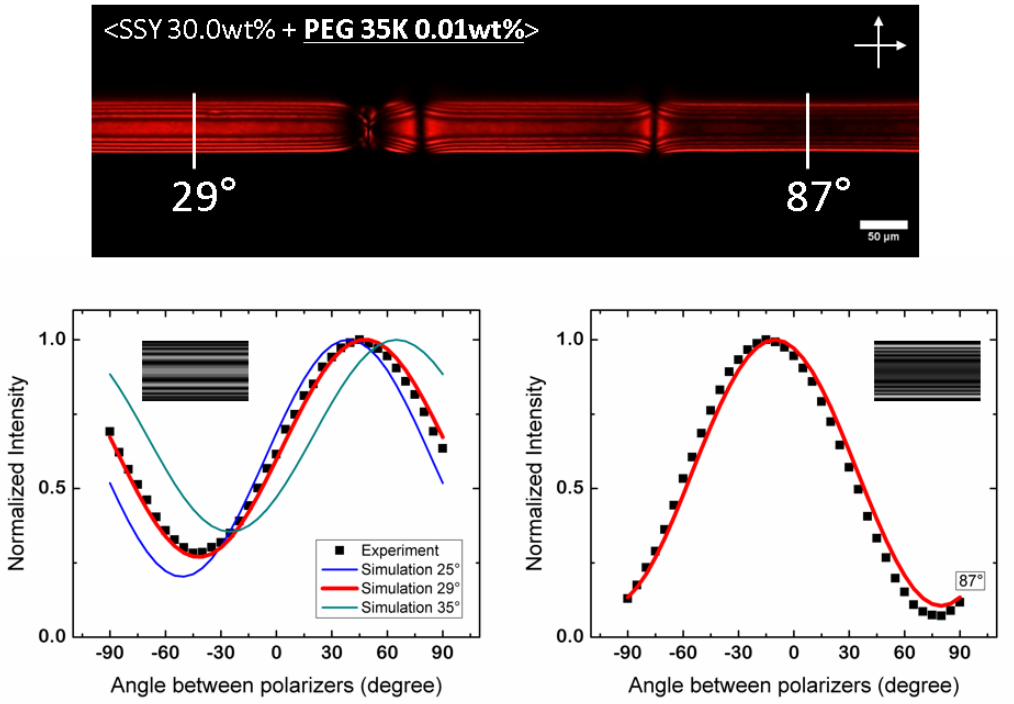

Figure S2. Twist angle estimation. The twist angles of a region marked with white lines are estimated and the resultant twist angles are written respectively. A wide rectangle with height of 10% of a capillary size is designated around the region laterally as the spot of intensity profile measurement. The intensity profiles from the experiments are denoted with black squares in the graphs. The colored lines are the intensity profiles from the numerically generated simulation and the red line is the best matched. As a final step, 2D optical texture employing the best matcher's parameters is compared to the experimental image. The inset images are the simulated images.

Code 1

```
ClearAll["`*"];

(* input *)
modeltype = 2(* 1 => linear / 2 => PRE *);
wavelen = 0.660; (* in micron *)
navg=1.42;
k2=1/10; (* K2/K3 *)

(* Dataset
filepath="Enter the location of stored data";
*)
filepath="D:\\Dropbox\\MyResearch\\twistangledata\\ID 50um PEG001_unsorted_simul1.txt";
inputexpdataorig=ReadList[filepath,Number,RecordLists->True];
inputexpdatadiameterset=inputexpdataorig[[1]];
inputexpdataset=Transpose[Drop[inputexpdataorig,1]];



nbifrstart=-0.090;nbifrend=-0.050;nbifrstep=0.0005;

(* Twist angle bottom to top. Enter positive vals only. Then code will search from -twistend to -
twiststart and from twiststart to twistend. *)
twiststart=(10*2)/180*Pi/2;twistend=(89*2)/180*Pi/2;twiststep=1/180*Pi;
polangstart=-
90/180*Pi;polangend=90/180*Pi;polangstep=5/180*Pi;polanglstepdeg=polangstep/Pi*180;
analyzerangle[angle_]:=0;

show3dvectorplot=False;showcenterintplotonly = True; showprogressbar = True;
```

Code 2

```
ClearAll["`*"];
starttime=SessionTime[];

(* input *)
modeltype = 2(* 1 => linear / 2 => PRE *);
polangstart=90/180*Pi;polangend=90/180*Pi;polangstep=5/180*Pi;
analyzerangle[angle_]:=0/180*Pi; (* for an arbitrary FIXED analyzerangle *)
k2=1/10; (* K2/K3 *)

wavelen = 0.660; (* in micron *)
navg=1.42;
systemradius = (52.13)/2; (* in micron *)

findresultorig={
    {({
        {-0.053`},
        {-43.`},
        {9.`}
       }), ({
        {-0.08600000000000001`},
        {51.`},
        {14.`}
       }), ({
        {-0.053`},
        {-42.`},
        {20.`}
       })}
  };
findresult=findresultorig[[1]];inputsize=Length[findresult];
nbifr=findresult[[1]][[1]];
twistangle=findresult[[1]][[2]]/180*Pi;

show3dvectorplot=False;showcenterintplotonly = False;showprogressbar = False;
```

Reference

[1] J. Lydon, "Chromonic liquid crystal phases," *Curr. Opin. Colloid Interface Sci.*, vol. 3, no. 5, pp. 458–466, 1998.

[2] S.-W. Tam-Chang and L. Huang, "Chromonic liquid crystals: properties and applications as functional materials," *Chem. Commun.*, no. 17, p. 1957, 2008.

[3] A. J. Dickinson, N. D. Laracuente, C. B. McKitterick, and P. J. Collings, "Aggregate structure and free energy changes in chromonic liquid crystals," *Mol. Cryst. Liq. Cryst.*, vol. 509, no. 1, pp. 9–20, 2009.

[4] D. J. Edwards, J. W. Jones, O. Lozman, A. P. Ormerod, M. Sintyureva, and G. J. T. Tiddy, "Chromonic liquid crystal formation by edicol sunset yellow," *J. Phys. Chem. B*, vol. 112, no. 46, pp. 14628–14636, 2008.

[5] H. S. Park *et al.*, "Self-assembly of Lyotropic chromonic liquid crystal sunset yellow and effects of ionic additives," *J. Phys. Chem. B*, vol. 112, no. 51, pp. 16307–16319, 2008.

[6] L. Tortora and O. D. Lavrentovich, "Chiral symmetry breaking by spatial confinement in tactoidal droplets of lyotropic chromonic liquid crystals," *Proc. Natl. Acad. Sci.*, vol. 108, no. 13, pp. 5163–5168, 2011.

[7] S. Zhou *et al.*, "Elasticity of lyotropic chromonic liquid crystals probed by director reorientation in a magnetic field," *Phys. Rev. Lett.*, vol. 109, no. 3, 2012.

[8] S. Zhou *et al.*, "Elasticity, viscosity, and orientational fluctuations of a lyotropic chromonic nematic liquid crystal disodium cromoglycate.," *Soft Matter*, vol. 10, no. 34, pp. 6571–81, 2014.

[9] J. Jeong, Z. S. Davidson, P. J. Collings, T. C. Lubensky, and A. G. Yodh, "Chiral symmetry breaking and surface faceting in chromonic liquid crystal droplets with giant elastic anisotropy," *Proc. Natl. Acad. Sci.*, vol. 111, no. 5, pp. 1742–1747, Feb. 2014.

[10] J. Fu, K. Nayani, J. O. Park, and M. Srinivasarao, "Spontaneous emergence of twist and the formation of a monodomain in lyotropic chromonic liquid crystals confined to capillaries," *NPG Asia Mater.*, vol. 9, no. 6, p. e393, 2017.

[11] Z. S. Davidson *et al.*, "Chiral structures and defects of lyotropic chromonic liquid crystals induced by saddle-splay elasticity," *Phys. Rev. E*, vol. 91, no. 5, pp. 1–5, 2015.

[12] R. D. Polak, G. P. Crawford, B. C. Kostival, J. W. Doane, and S. Umer, "Optical determination of the saddle-splay elastic constant K24 in nematic liquid crystals," *Phys. Rev. E*, vol. 49, no. 2, 1994.

[13] K. Nayani *et al.*, "Spontaneous emergence of chirality in achiral lyotropic chromonic liquid crystals confined to cylinders," *Nat. Commun.*, vol. 6, p. 8067, Aug. 2015.

[14] S. Zhou, A. Sokolov, O. D. Lavrentovich, and I. S. Aranson, "Living liquid crystals.," *Proc. Natl. Acad. Sci. U. S. A.*, vol. 111, no. 4, pp. 1265–70, 2014.

[15] Y. A. Nastishin *et al.*, "Optical characterization of the nematic lyotropic chromonic liquid crystals: Light absorption, birefringence, and scalar order parameter," *Phys. Rev. E - Stat. Nonlinear, Soft Matter Phys.*, vol. 72, no. 4, pp. 1–14, 2005.

[16] S. V. Shiyanovskii *et al.*, "Real-time microbe detection based on director distortions around growing immune complexes in lyotropic chromonic liquid crystals," *Phys. Rev. E - Stat. Nonlinear, Soft Matter Phys.*, vol. 71, no. 2, pp. 1–4, 2005.

[17] T. K. Attwood, J. E. Lydon, C. Hall, and G. J. T. Tiddy, "The distinction between chromonic and amphiphilic lyotropic mesophases," *Liq. Cryst.*, vol. 7, no. 5, pp. 657–668, May 1990.

[18] L. J. Yu and A. Saupe, "Deuteron Resonance of D2O of Nematic Disodium Cromoglycate-Water Systems," *Mol. Cryst. Liq. Cryst.*, vol. 80, no. 1, pp. 129–134, Feb. 1982.

[19] J. P. De Almeida Martins, F. V. Chávez, and P. J. Sebastião, "NMR molecular dynamics study of chromonic liquid crystals Edicol Sunset Yellow doped with salts," *Magn. Reson. Chem.*, vol. 52, no. 10, pp. 540–545, 2014.

[20] D. Perahia, D. Goldfarb, and Z. Luz, "Sodium-23 NMR in the Lyomesophases of Disodium cromoglycate," *Mol. Cryst. Liq. Cryst.*, vol. 108, no. 1–2, pp. 107–123, Jun. 1984.

[21] S. Zhou, "Lyotropic Chromonic Liquid Crystals," 2017.

[22] O. P. Boiko, R. M. Vasyuta, O. M. Semenyshyn, Y. A. Nastishin, and V. G. Nazarenko, "Chromonic nematic phase and scalar order parameter of indanthrone derivative with ionic additives," *Ukr. J. Phys. Opt.*, vol. 9, no. 4, pp. 236–246, 2008.

[23] L. Tortora *et al.*, "Self-assembly, condensation, and order in aqueous lyotropic chromonic liquid crystals crowded with additives," *Soft Matter*, vol. 6, no. 17, pp. 4157–4167, 2010.

[24] S. K. Prasad, G. G. Nair, G. Hegde, and Y. Jayalakshmi, "Evidence of wormlike micellar behavior in chromonic liquid crystals: Rheological, X-ray, and dielectric studies," *J. Phys. Chem. B*, vol. 111, no. 33, pp. 9741–9746, 2007.

[25] A. P. Ormerod, J. W. Jones, H. Wheatcroft, A. Alfutimie, and G. J. T. Tiddy, "The influence of polar additives on chromonic mesophase formation of Edicol Sunset Yellow," *Liq. Cryst.*, vol. 42, no. 5–6, pp. 772–782, 2015.

[26] A. F. Kostko *et al.*, "Salt effects on the phase behavior, structure, and rheology of chromonic liquid crystals," *J. Phys. Chem. B*, vol. 109, no. 41, pp. 19126–19133, 2005.

[27] L. Wu, J. Lal, K. A. Simon, E. A. Burton, and Y. Y. Luk, "Nonamphiphilic assembly in water: Polymorphic nature, thread structure, and thermodynamic incompatibility," *J. Am. Chem. Soc.*, vol. 131, no. 21, pp. 7430–7443, 2009.

[28] H. Von Berlepsch and C. Böttcher, "Network superstructure of pseudoisocyanine J-aggregates in aqueous sodium-chloride solution revealed by cryo-transmission electron microscopy," *J.*

Phys. Chem. B, vol. 106, no. 12, pp. 3146–3150, 2002.

[29] B. Zhang and H. S. Kitzerow, "Influence of Proton and Salt Concentration on the Chromonic Liquid Crystal Phase Diagram of Disodium Cromoglycate Solutions: Prospects and Limitations of a Host for DNA Nanostructures," *J. Phys. Chem. B*, vol. 120, no. 12, pp. 3250–3256, 2016.

[30] A. Alfutimie, A. P. Ormerod, D. J. Edwards, G. J. T. Tiddy, H. Wheatcroft, and J. W. Jones, "The influence of sodium chloride and urea on chromonic liquid crystals formed by CI Acid Red 266," *Liq. Cryst.*, vol. 42, no. 11, pp. 1519–1526, Nov. 2015.

[31] A. P. O. Unilever, "Aggregation and lyotropic liquid crystal formation of anionic azo dyes for textile fibres," vol. 28, no. April, pp. 2–3, 2015.

[32] J. W. Jones, L. Lue, A. P. Ormerod, and G. J. T. Tiddy, "The influence of sodium chloride on the self-association and chromonic mesophase formation of Edicol Sunset Yellow," *Liq. Cryst.*, vol. 37, no. 6–7, pp. 711–722, Jul. 2010.

[33] B. Neumann, "On the aggregation behavior of pseudoisocyanine chloride in aqueous solution as probed by UV/vis spectroscopy and static light scattering," *J Phys Chem B*, vol. 105, no. 34, pp. 8268–8274, 2001.

[34] L. Spindler, I. Drevenšek-Olenik, M. Čopič, J. Cerar, J. Škerjanc, and P. Mariani, "Dynamic light scattering and 31P NMR study of the self-assembly of deoxyguanosine 5′-monophosphate: The effect of added salt," *Eur. Phys. J. E*, vol. 13, no. 1, pp. 27–33, 2004.

[35] Bahr, Christian, and Heinz-Siegfried Kitzerow. *Chirality in liquid crystals*. Heidelberg: Springer, 2001.

[36] H. Lee and M. M. Labes, "Lyotropic Cholesteric and Nematic Phases of Disodium Cromoglycate in Magnetic Fields," *Mol. Cryst. Liq. Cryst.*, vol. 84, no. 1, pp. 137–157, 1982.

[37] P. D. E. Un *et al.*, "Treball Final de Grau," vol. 1, no. June, p. 300, 2016.

[38] T. Ogolla, S. B. Nashed, and P. J. Collings, "Pitch measurements in chiral lyotropic chromonic liquid crystals," *Liq. Cryst.*, vol. 44, no. 12–13, pp. 1968–1978, 2017.

[39] L. Bergquist and T. Hegmann, "Chiral Amplification by L-Cysteine-Capped Gold Nanoparticles in Lyotropic Chromonic Liquid Crystals," *ChemNanoMat*, vol. 3, no. 12, pp. 863–868, 2017.

[40] F. Berride *et al.*, "Chiral amplification of disodium cromoglycate chromonics induced by a codeine derivative," *Soft Matter*, vol. 13, no. 38, pp. 6810–6815, 2017.

[41] T. Shirai *et al.*, "Chiral lyotropic chromonic liquid crystals composed of disodium cromoglycate doped with water-soluble chiral additives," *Soft Matter*, vol. 14, no. 9, pp. 1511–1516, 2018.

[42] D. Goldfarb, M. E. Moseley, M. M. Labes, and Z. Luz, "Determination of Pitch in a Cholesteric DSCG-Water Lyomesophase by NMR Techniques," *Mol. Cryst. Liq. Cryst.*, vol.

89, no. 1–4, pp. 119–135, Oct. 1982.

[43] H. Lee and M. M. Labes, “Helical Twisting Power of Amino Acids in a Nematic Lyophase,” *Mol. Cryst. Liq. Cryst.*, vol. 108, no. 1–2, pp. 125–132, Jun. 1984.

[44] M. Lavrentovich, T. Sergan, and J. Kelly, “Planar and twisted lyotropic chromonic liquid crystal cells as optical compensators for twisted nematic displays,” *Liq. Cryst.*, vol. 30, no. 7, pp. 851–859, 2003.

[45] M. Lavrentovich, T. Sergan, and J. Kelly, “Lyotropic chromonic liquid crystals for optical applications - An optical retardation plate for twisted nematic cells,” *Mol. Cryst. Liq. Cryst.*, vol. 409, pp. 21–28, 2004.

[46] Q. Li, *Liquid Crystals Beyond Displays: Chemistry, Physics, and Applications*. Wiley, 2012.

[47] C. K. McGinn, L. I. Laderman, N. Zimmermann, H.-S. Kitzerow, and P. J. Collings, “Planar anchoring strength and pitch measurements in achiral and chiral chromonic liquid crystals using 90-degree twist cells,” *Phys. Rev. E*, vol. 88, no. 6, p. 062513, Dec. 2013.

[48] S. Yang *et al.*, “Stereochemical control of nonamphiphilic lyotropic liquid crystals: Chiral nematic phase of assemblies separated by six nanometers of aqueous solvents,” *J. Phys. Chem. B*, vol. 117, no. 23, pp. 7133–7143, 2013.

[49] C. Peng and O. D. Lavrentovich, “Chirality amplification and detection by tactoids of lyotropic chromonic liquid crystals,” *Soft Matter*, vol. 11, no. 37, pp. 7257–7263, 2015.

[50] L. Tortora and O. D. Lavrentovich, “Chiral symmetry breaking by spatial confinement in tactoidal droplets of lyotropic chromonic liquid crystals,” *Proc. Natl. Acad. Sci.*, vol. 108, no. 13, pp. 5163–5168, Mar. 2011.

[51] H. S. Park, S. W. Kang, L. Tortora, S. Kumar, and O. D. Lavrentovich, “Condensation of self-assembled lyotropic chromonic liquid crystal sunset yellow in aqueous solutions crowded with polyethylene glycol and doped with salt,” *Langmuir*, vol. 27, no. 7, pp. 4164–4175, 2011.

[52] K. Nayani, J. Fu, R. Chang, J. O. Park, and M. Srinivasarao, “Using chiral tactoids as optical probes to study the aggregation behavior of chromonics,” *Proc. Natl. Acad. Sci.*, p. 201614620, 2017.

[53] P. J. Collings, P. van der Asdonk, A. Martinez, L. Tortora, and P. H. J. Kouwer, “Anchoring strength measurements of a lyotropic chromonic liquid crystal on rubbed polyimide surfaces,” *Liq. Cryst.*, vol. 44, no. 7, pp. 1165–1172, 2017.

[54] P. van der Asdonk, P. J. Collings, and P. H. J. Kouwer, “Fully Stable and Homogeneous Lyotropic Liquid Crystal Alignment on Anisotropic Surfaces,” *Adv. Funct. Mater.*, vol. 27, no. 28, pp. 1–10, 2017.

[55] A. Yamaguchi *et al.*, “Phases and structures of sunset yellow and disodium cromoglycate mixtures in water,” *Phys. Rev. E - Stat. Nonlinear, Soft Matter Phys.*, vol. 93, no. 1, pp. 1–7, 2016.

[56] V. R. Horowitz, L. A. Janowitz, A. L. Modic, P. A. Heiney, and P. J. Collings, "Aggregation behavior and chromonic liquid crystal properties of an anionic monoazo dye," *Phys. Rev. E - Stat. Nonlinear, Soft Matter Phys.*, vol. 72, no. 4, pp. 1–10, 2005.

[57] R. L. Parfitt and D. J. Greenland, "The Adsorption of Poly(Ethylene Glycols) on Clay Minerals," *Clay Miner.*, vol. 8, no. 03, pp. 305–315, 1970.

[58] Park, Heung-Shik. *Self-assembly of lyotropic chromonic liquid crystals: Effects of additives and applications*. Diss. Kent State University, 2010.

Acknowledgment

I thank my advisor Prof. Joonwoo Jeong from the bottom of my heart. He has taught me not only how to plan and do an experiment but also how to be a good person. I thank SOPHY members: Dr. Sungjo Kim, Dr. Eujin Um, Jonghee Eun, Jackwan Im, Hyewon Kang, Leekyo Jung, Jungmyung Kim, and Minjun Kim. I will always cherish every memory with you. Especially, I thank Jonghee a lot for taking care of me like a sister when I had gone through tough times. I thank my friends, Suhyun Han, Juran Moon, and Hanseul Kim for making my days in school full of laughs and joy. I thank my family and friends in my hometown for encouraging me relentlessly. Lastly, I thank the school for giving me such a privilege to be educated for years.

I have been so lucky to be a part of SOPHY. I thank you all SOPHY members.